อุปกรณ์ขับเคลื่อนด้วยพลังงานแสงจากเลดเซอร์โคเนตไททาเนต ที่ดัดแปรด้วยแลนทานัม

นายภาณุ เวทยนุกูล

วิทยานิพนธ์นี้เป็นส่วนหนึ่งของการศึกษาตามหลักสูตรปริญญาวิทยาศาสตรมหาบัณฑิต
สาขาวิชาเทคโนโลยีเซรามิก ภาควิชาวัสดุศาสตร์
คณะวิทยาศาสตร์ จุฬาลงกรณ์มหาวิทยาลัย
ปีการศึกษา 2543

ISBN 974-13-0296-7

LANTHANUM-MODIFIED LEAD ZIRCONATE TITANATE PHOTOSTRICTIVE ACTUATORS

Mr.Bhanu Vetayanugul

A Thesis Submitted in Partial Fulfillment of the Requirements
for the Degree of Master of Science in Ceramic Technology
Department of Materials Science
Faculty of Science
Chulalongkorn University
Academic Year 2000

ISBN 974-13-0296-7

Thesis Title	LANTHANUM-MODIFIED LEAD ZIRCONATE TITANATE PHOTOSTRICTIVE ACTUATORS
By	Bhanu Vetayanugul
Field of Study	Ceramic Technology
Thesis Advisor	Associate Professor Supatra Jinawath, Ph.D.
Thesis Co-advisor	Patcharin Burke, Ph.D.

Accepted by the Faculty of Science, Chulalongkorn University in Partial Fulfillment of the Requirements for the Master's Degree

……..Dean of Faculty of Science
(Associate Professor Wanchai Phothiphichitr, Ph.D.)

THESIS COMMITTEE

…….. Chairman
(Associate Professor Saowaroj Chuayjuljit)

…….. Thesis Advisor
(Associate Professor Supatra Jinawath, Ph.D.)

…….. Thesis Co-advisor
(Patcharin Burke, Ph.D.)

…….. Member
(Assistant Professor Sutin Kuharuangrong, Ph.D.)

…….. Member
(Sirithan Jiemsirilers, Ph.D.)

ภาณุ เวทยนุกูล : อุปกรณ์ขับเคลื่อนด้วยพลังงานแสงจากเลดเซอร์โคเนตไททาเนต
ที่ดัดแปรด้วยแลนทานัม. (LANTHANUM-MODIFIED LEAD ZIRCONATE TITANATE
PHOTOSTRICTIVE ACTUATORS) อ. ที่ปรึกษา : รศ.ดร.สุพัตรา จินาวัฒน์,
อ. ที่ปรึกษาร่วม : ดร.พัชรินทร์ เบอร์ค, 79 หน้า. ISBN 974-13-0296-7.

การผลิตแอคชูเอเตอร์ให้มีขนาดเล็กลงอย่างต่อเนื่องเป็นผลให้แอคชูเอเตอร์ที่ขับเคลื่อนด้วยแสงมีนัยสำคัญยิ่งขึ้นในการที่จะพัฒนาเป็นเครื่องมือขนาดจุลภาคในอนาคต งานวิจัยนี้ได้ทำการศึกษาเพื่อเพิ่มประสิทธิภาพของสารโฟโตสตริกทีฟเลดเซอร์โคเนตไททาเนตที่ดัดแปรด้วยแลนทานัม (PLZT) สัดส่วนองค์ประกอบ 3/52/48 4/48/52 และ 5/54/46 โดยการเจือ Nb_2O_5 และ Gd_2O_3

จากการทดลองพบว่า PLZT 4/48/52 ให้ค่าโฟโตเคอร์เรนท์สูงที่สุดจึงนำมาประกอบเป็นตัวจ่ายกระแสไฟฟ้าโดยใช้การต่อชิ้นงานแบบขนานเพื่อเพิ่มกระแสให้มากขึ้น ในขณะที่ PLZT 5/54/46 ซึ่งเติมด้วย Nb_2O_5 0.5 เปอร์เซ็นต์โดยอะตอมมีค่าคงที่ไดอิเล็กทริก ค่าคงที่เพียโซอิเล็กทริก โฟโตโวลเทจ โฟโตอิน-ดิวซ์สเตรนสูงสุด จึงถูกนำมาประกอบเป็นหุ่นยนต์ขับเคลื่อนด้วยแสงโดยใช้การต่อชิ้นงานแบบอนุกรมเพื่อเพิ่มโฟโตโวลเทจให้มากขึ้น

ภาควิชา วัสดุศาสตร์	ลายมือชื่อนิสิต .....
สาขาวิชา เทคโนโลยีเซรามิก	ลายมือชื่ออาจารย์ที่ปรึกษา.....
ปีการศึกษา 2543	ลายมือชื่ออาจารย์ที่ปรึกษาร่วม.....

4272364623 : MAJOR Ceramic Technology

KEY WORD : photostrictive/ photovoltaic/ photovoltage/ photocurrent/ actuators

BHANU VETAYANUGUL : LANTHANUM-MODIFIED LEAD ZIRCONATE TITANATE PHOTOSTRICTIVE ACTUATORS.

THESIS ADVISOR : Associate Professor Supatra Jinawath, Ph.D.,

THESIS CO-ADVISOR : Patcharin Burke, Ph.D. 79 pp. ISBN 974-13-0296-7.

With the decreasing in size of miniature actuators, a photostrictive actuator becomes more significant and promising for future micro-devices. In this study, the optimization of photostrictive PLZT 3/52/48, 4/48/52 and 5/54/46 ceramics through doping with Nb_2O_5 and Gd_2O_3 was investigated.

Undoped PLZT (4/48/52) ceramic provided the maximum photocurrent and was fabricated into a power supply device using a parallel circuit to increase the generated current.

PLZT (5/54/46) doped with 0.5 at% Nb_2O_5 displayed the highest values of dielectric constant, piezoelectric constant, photovoltage and photo-induced strain. It was fabricated into a micro-walker using a series circuit of which the generated photovoltage in each PLZT sample was combined and displayed the total value.

Department Materials Science	Student's signature ……..……
Field of study Ceramic Technology	Advisor's signature ……..……
Academic year 2000	Co-advisor's signature ……

Acknowledgement

I would like to express my gratitude to my thesis advisor, Associate Professor Dr. Supatra Jinawath and co-advisor, Dr. Patcharin Burke, for their help and guidance throughout the course of the study. I especially thank Dr. patcharin Burke who graciously gave her time to correct and comment on the detail of this thesis and her generous help makes this thesis possible.

My sincere appreciation goes to my thesis committee: Associate Professor Saowaroj Chuayjuljit, Assistant Professor Dr. Sutin Kuharuangrong and Dr.Sirithan Jiemsirilers, for their valuable comments and suggestions.

I am greatly indebted to the Department of Physics at Chulalongkorn University for the permission to use the poling equipment. I also would like to express my special thanks to the technical staff at Thailand Institute of Science and Technological Research (TISTR) and Metal and Materials Technology Center (MTEC) for their help with scientific instruments.

I also wish to thank Thailand Graduate Institute of Science and Technology (TGIST) for the graduate scholarship and National Metal and Materials Technology Center (MTEC) for the research facilities.

Furthermore, I would like to express my sincere gratitude to my parents for their love, hearty encouragement during my study. Without them my thesis would have never been accomplished.

I truly believe that all people whom I have not personally mentioned here are aware of my deep appreciation.

CONTENTS

Page

Abstract (Thai).....iv

Abstract (English).....v

Acknowledgements.....vi

Contents.....vii

List of tables.....ix

List of Figures.....x

Chapter 1 Introduction.....1

Chapter 2 Literature Review.....3

2.1 Photostrictive Effect.....3

2.2 PLZT compositional system.....6

2.3 Effect of compositions on PLZT properties.....7

2.4 Effect of dopants on PLZT properties.....10

2.5 Effect of grain size on PLZT properties.....14

2.6 Applications based on Photovoltaic and Photostrictive Effects....16

2.7 Examples of Photostrictive and Piezoelectric devices.....17

2.7.1 Photo-acoustic device (Photophone).....17

2.7.2 Piezoelectric buzzer.....18

2.7.3 Micro walking device.....19

2.7.4 The light source chasing device.....21

Chapter 3 Experimental work.....23

3.1 Preparation of Powders and Polycrystalline samples.....23

3.2 Characterization of Ceramic Specimens.....27

3.2.1 Phase Analysis of PLZT powders.....27

3.2.2 Microstructure Analysis.....27

3.2.3 Bulk Density and Relative Density of Sintered Samples.....27

Page

3.2.4 Dielectric and Piezoelectric properties 29
3.2.4.1 Dielectric properties 29
3.2.4.2 Piezoelectric properties 29
3.2.5 Photovoltage and Photocurrent Measurement 29
3.3 Fabrication of Photostrictive devices 31

Chapter 4 Results and discussion 32
4.1 Phase analysis of PLZT samples 32
4.2 Microstructure Analysis 37
4.3 Bulk Density, and Relative Density of sintered samples 44
4.4 Dielectric and Piezoelectric properties 45
4.4.1 Dielectric properties 45
4.4.2 Piezoelectric properties 46
4.5 Photovoltage and Photocurrent Measurement 48
4.6 Fabrication of photostrictive devices 55
4.6.1 Photocurrent power supply 55
4.6.2 Micro-walker device 57
Chapter 5 Conclusions 60
Chapter 6 Suggestions for future works 62
References 63
Appendices 66
Appendix A 68
Appendix B 72
Appendix C 77
Vita 79

LISTS OF TABLES

Page

Table 3.1 Component oxide powders used in the synthesis of PLZT ceramics by a conventional oxide mixing process.....24

Table 4.1 Lattice parameters, tetragonality, and unit cell volume of the sintered PLZT samples (calculated from the XRD patterns).....36

Table 4.2 The average grain sizes of PLZT samples depending on composition and type of dopants 38

Table 4.3 Bulk density and Relative density of sintered PLZT samples....44

Table 4.4 Room temperature dielectric constant and the dissipation factor of the PLZT samples.....45

Table 4.5 Piezoelectric constant (d_{33}) of PLZT samples.....46

Table 4.6 photocurrent and photovoltage of PLZT samples (Light intensity 2.1 mW/cm^2) 48

Table 4.7 The merit of response speed and magnitude of strain.....54

LIST OF FIGURES

Page

Fig.2.1 The schematic diagram of photostrictive effect.....4

Fig.2.2 Perovskite ABO_3 ionic structure of PLZT system 7

Fig.2.3 Room temperature phase diagram of the PLZT system.....8

Fig.2.4 The contour map for response speed of PLZT system
PLZT 4/48/52 showed the highest response speed.....9

Fig.2.5 The contour map for photo-induced strain of PLZT system
PLZT 5/54/46 showed the maximum value.....10

Fig.2.6 Photovoltaic effect with various dopants (1 at% content) in
PLZT (3/52/48) ceramics.....12

Fig.2.7 Photostriction and photovoltage as functions of various
dopants (1 at% content) in PLZT (3/52/48) ceramics.....13

Fig.2.8 Grain size dependence of photostrictive characteristics
in PLZT (3/52/48) after Sada et al. (1987).....14

Fig.2.9 Grian size dependence of a) piezoelectric constant
b) tetragonality.....15

Fig.2.10 Experimental setup for photo-induced mechanical resonance
using an optical chopper.....18

Fig.2.11 Piezoelectric Buzzer.....19

Fig.2.12 a) Arch-shaped type photoactuating film composites
b) The triangular top shape photoactuating film composites...20

Fig.2.13 a) The light source chasing device based on
photoactuating film composites
b) schematic diagram of the device movement.....21

Fig.3.1 The conventional oxide mixing flow chart of PLZT ceramics.....25

Page

Fig.3.2 The calcination step for preparation of PLZT ceramics.....26

Fig.3.3 The sintering step for preparation of PLZT ceramics.....26

Fig.3.4 The schematic diagram for photovoltage and the photocurrent measuring system.....30

Fig.3.5 Photocurrent measured as a function of applied voltage.....31

Fig.4.1 XRD patterns of PLZT (3/52/48) powder and sintered ceramics calcined at different temperatures.....33

Fig.4.2 XRD patterns of undoped and doped PLZT (3/52/48) ceramics.....34

Fig.4.3 XRD patterns of undoped and doped PLZT (4/48/52) ceramics.....34

Fig.4.4 XRD patterns of undoped and doped PLZT (5/54/46) ceramics.....35

Fig.4.5 PLZT compositional contour map.....37

Fig.4.6 The effect of composition and dopants on the average grain size.....38

Fig.4.7 SEM micrograph of undoped PLZT (3/52/48) ceramic.....39

Fig.4.8 SEM micrograph of 0.5 at% Gd_2O_3 doped PLZT (3/52/48) ceramic.....40

Fig.4.9 SEM micrograph of 0.5 at% Nb_2O_5 doped PLZT (3/52/48) ceramic.....40

Fig.4.10 SEM micrograph of undoped PLZT (4/48/52) ceramic.....41

Fig.4.11 SEM micrograph of 0.5 at% Gd_2O_3 doped PLZT (4/48/52) ceramic.....41

Fig.4.12 SEM micrograph of 0.5 at% Nb_2O_5 doped PLZT (4/48/52) ceramic.....42

Page

Fig.4.13 SEM micrograph of undoped PLZT (5/54/46) ceramic.....42

Fig.4.14 SEM micrograph of 0.5 at% Gd_2O_3 doped PLZT (5/54/46) ceramic 43

Fig.4.15 SEM micrograph of 0.5 at% Nb_2O_5 doped PLZT (5/54/46) ceramic 43

Fig.4.16 The relation between dielectric constant (K) and piezoelectric constant (d_{33}) of poled PLZT samples.....47

Fig.4.17 I_{ph} as a function of E_{ph} in PLZT samples.....50

Fig.4.18 I_{ph} as a function of G_{ph} in PLZT samples.....51

Fig.4.19 E_{ph} as a function of G_{ph} in PLZT samples.....52

Fig.4.20 Iph as a function of Tetragonality.....53

Fig.4.21 The design of photocurrent power supply and its equivalent circuit.....56

Fig.4.22 The design of micro-walker's body.....57

Fig.4.23 The design of micro-walker device.....58

CHAPTER 1
INTRODUCTION

Actuators are defined as the transducers which can transduce an input energy into a mechanical output energy. These devices can be designed to move, rotate, or drive things dynamically when an input energy is applied, which make them widely used in a broad spectrum of technologies such as in optics, astronomy, fluid control or precision machining.

The conventional actuators are categorized into three types according to their driving sources as an air pressure, oil pressure, and electrical-controlled types. Both air and oil pressure-controlled actuators are large in size and slow in response speed. To miniaturize the size of the actuators and to increase the response speed, the electrical-controlled type actuators are preferred and promising .

In recent years, the need for new displacement actuators has increased significantly in many fields due to the requirement of high accuracy and micro-positioning actuators, which lead to the discovery and usage of piezoelectric and electrostrictive actuators. Piezoelectric actuators, which strain induced by an applied electric field, are developed for such applications, i.e. vibrators, buzzers, speakers, sensors and ultrasonic generators. However, due to the weight of the electrical lead wire, it is almost impossible for the piezoelectric actuators to be used for sub-millimeter devices of which the connecting lead wire will become significant. Therefore the research area has been moved to a new promising candidate, the wireless photo-driven actuators which were activated and driven by incident light, *"Photostrictive Actuators".*

Photostrictive effect is the combination of photovoltaic, i.e. generation of large voltage from the irradiation of light, and converse-piezoelectric effect, i.e. expansion or contraction under the applied voltage. This effect has the ability to convert light directly into the physical movement. When the photostrictive materials are uniformly illuminated, a large voltage of the order of kv/cm is generated. Along with this photovoltage, mechanical strain is also induced due to the converse-piezoelectric effect. This effect has been observed in non-centrosymmetric materials such as ferroelectric single crystals or ferroelectric polycrystalline materials. Because of relatively high piezoelectric coefficient, lanthanum-modified lead zirconate titanate (PLZT) ceramics is one of the most promising photostrictive materials for wireless photo-driven actuators.

The goal of this research is to fabricate the high induced strain and fast response speed PLZT ceramics, which can be achieved through the fabrication of PLZT ceramics with suitable composition and dopants by the conventional oxide mixing method. In addition a photostrictive device will be designed and fabricated. This photostrictive device will be a prototype for a micro devices which is small in size, inexpensive and have the ability to sense and get actuated itself. This research will couple electrical, optical and mechanical fields together and serve as a useful guideline for new materials, sensors and actuators.

CHAPTER 2
LITERATURE REVIEW

Photostrictive materials have received considerable attention in a broad spectrum of applications, especially in the area of microactuation and microsensing. The capability of directly producing strain by light illumination without any electrical lead wire connection makes them very attractive for decreasing in size and weight of actuators.

2.1 Photostrictive Effect

Photostrictive effect is the combination of photovoltaic, i.e. generation of high voltage from the irradiation of light, and piezoelectric effect, i.e. generation of electrical charge from a mechanical stress. This combination effect was studied and termed as "Photostriction" in 1982 by Uchino, Aizawa and Nomura. When an incident light, which has the energy equal to the materials band gap energy illuminates the photostrictive materials, a high voltage is generated. Along with this high voltage, mechanical strain is also induced due to the converse piezoelectric effect. The schematic diagram of photostrictive effect is displayed in Fig.2.1.

The photo-induced strain as a function of time (t) has been proposed by considering both response time and the magnitude of strain. This relation is given by Poosanaas P. and Uchino K. (1999)[1] as following :

$$X_{ph} = d_{33}E_{ph}\left[1 - \exp\left(\frac{-t}{RC}\right)\right] \qquad (2.1)$$

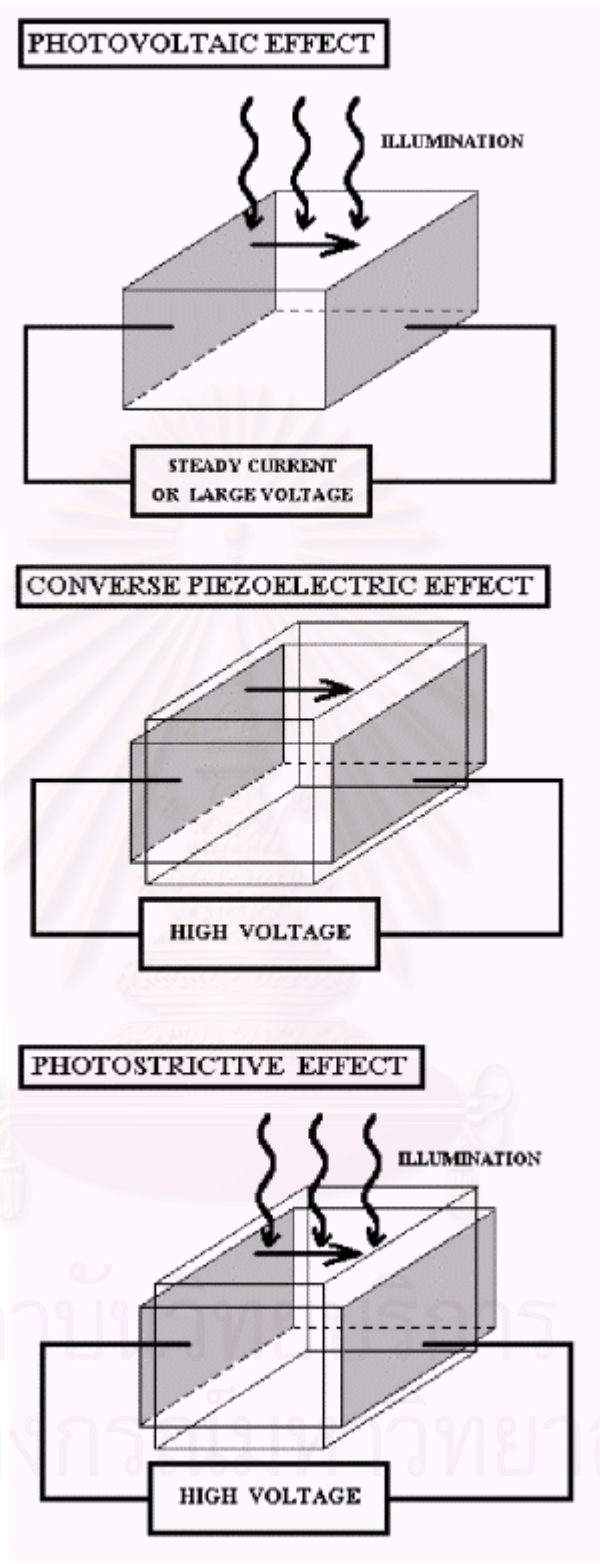

Fig.2.1 The schematic diagram of photostrictive effect

Where X_{ph} is the photo-induced strain

d_{33} is the piezoelectric constant of the materials

E_{ph} is the photovoltage

R and C are the resistance and the capacitance of the materials

From the above equation, if t <<1, we can obtain

$$X_{ph} = d_{33}E_{ph}\left(\frac{t}{RC}\right) = \left(\frac{d_{33}E_{ph}}{RC}\right)t \qquad (2.2)$$

Thus, the significant term for response speed should be provided by $\frac{d_{33}E_{ph}}{RC}$. Using the relation $I_{ph} = \frac{E_{ph}}{R}$, where I_{ph} is the photocurrent, equation (2.2) is then transformed to

$$X_{ph} = \left(\frac{d_{33}I_{ph}}{C}\right)t \qquad (2.3)$$

In order to obtain a high photo-induced strain, materials with high d_{33} and E_{ph} are needed. On the contrary, for high response speed, materials with high d_{33}, I_{ph}, and low dielectric constant (K) are required.

On the other hand, for t >> 1, equation (2.1) can be simplified to

$$X_{ph} = d_{33}E_{ph}$$

which is similar to the previous paper reported by Uchino K. et al.(1985)[1]

Photostrictive effect has been investigated in certain ferroelectric materials such as lanthanum-modified lead zirconate titanate. Transparent

lanthanum-modified lead zirconate titanate (PLZT) ceramics were developed in 1969 to increase the optical properties of conventional lead zirconate titanate (PZT) [Haertling and Land (1971)][(2)]. PLZT ceramic is a promising photostrictive material due to its relatively high piezoelectric constant (d_{33}) and ease of fabrication.

Significant improvements in the transparency and optical clarity of the PLZT materials were made within a year, through the development of

1. Hot-pressing technique
2. Chemical coprecipitation process
3. Sintering in PbO atmosphere

These techniques were developed to improve the materials quality for electro-optic applications [Haertling and Land (1972)][(3)].

2.2 PLZT compositional system

PLZT is a promising photostrictive material which also has excellent piezoelectric properties. The solid-solution system that forms the PLZT materials is a series of compositions resulting from the complete miscibility of lead zirconate and lead titanate in each other and modified by the solubility of substantial lanthanum oxide in the crystalline lattice.

A general formula for all compositions in PLZT (x/y/z) system is

$$Pb_{1-x}La_x(Zr_yTi_{1-y})_{1-x/4}O_3$$

where lanthanum ions replace lead ions in the A site of the perovskite ABO_3 as shown in Fig.2.2. Since La^{3+} substitutes for Pb^{2+}, electrical neutrality is maintained by the creation of lattice site vacancies. The formula above presumes that all the vacancies are in B sites[(4-7)].

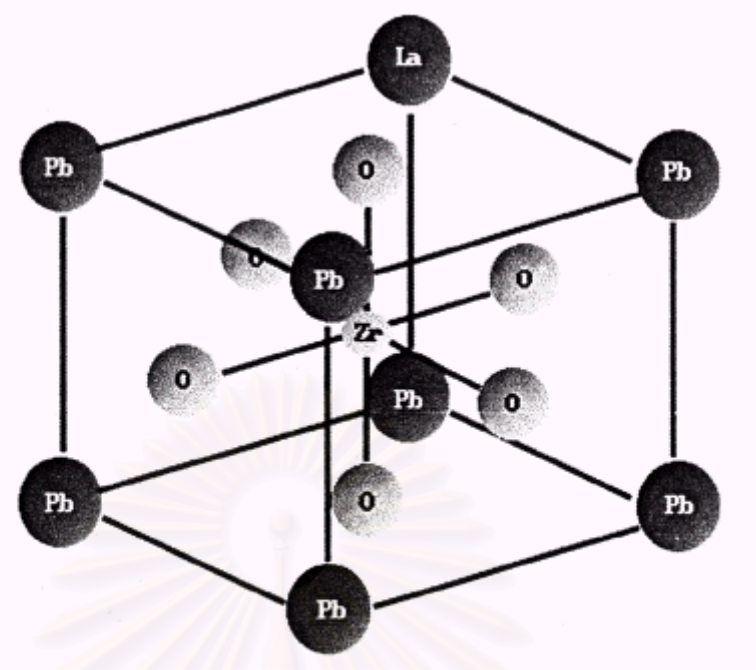

Fig.2.2 Perovskite ABO_3 ionic structure of PLZT system

2.3 Effect of compositions on PLZT properties

Depending upon the specific requirement for different applications of PLZT ceramics, various compositions may be developed. Dielectric, piezoelectric and photovoltaic properties are very significant properties for many applications. Therefore, materials that have optimum properties are required. In general, these optimum properties are found in materials with composition along the morphotropic phase boundaries (MPBs) which separate tetragonal and rhombohedral feroelectric phases. Room temperature phase diagram of the PLZT system is shown in Fig.2.3.

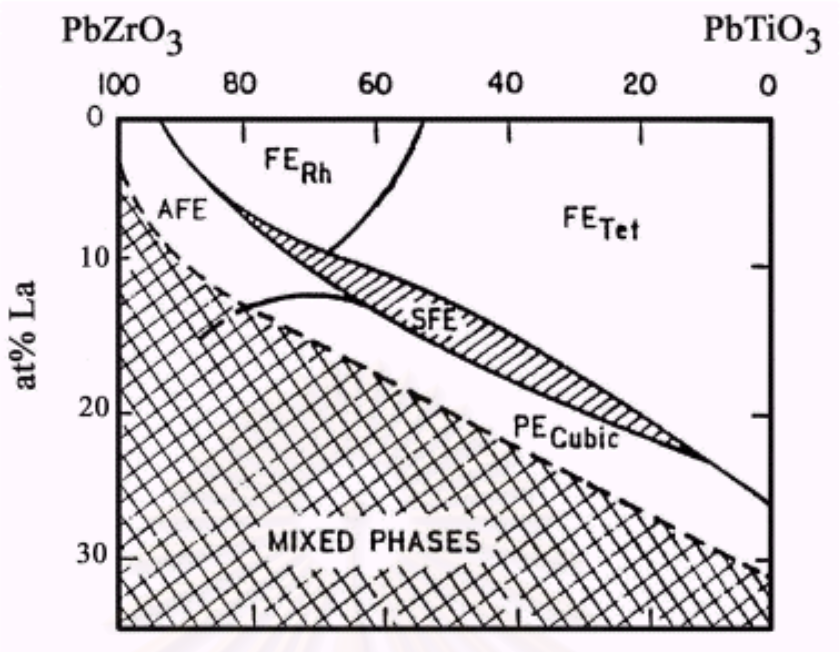

Fig.2.3 Room temperature phase diagram of the PLZT system [Haertling and Land (1971)][2]

There are many studies concentrated on the PZT and PLZT with composition along the morphotropic phase boundaries (MPBs). Meitzler A.H. and O'Bryan H.M., Jr.(1973)[8] suggested that PLZT X/65/35 system which closed to the MPBs generally possess properties useful in device applications. A high dielectric constant PLZT was found in composition 9/65/35 and the maximum reported value of d_{33} (710 pC/N) was found in composition 7/60/40, which located near the MPBs [Buchanan R.C. (1991)][4].

Tjhen W. et al. (1991)[9] studied PZT thin film and reported that 54/46 PZT thin films exhibited a useful combination of ferroelectric, pyroelectric and piezoelectric properties. This paper reported the dielectric and piezoelectric constants in the range of 500-3400 and 155-590 pC/N, respectively.

Among a lot of studies in PZT and PLZT compositions, PZT 52/48 and PLZT x/52/48 were promising. PZT thin film with composition 52/48 was found to have a high remanant polarization. Nonaka K. et al. reported that the highest photostrictive efficiency had been obtained with the composition (3/52/48) [Nonaka K. et al.(1995)][10].

Uchino K. (1997)[11] indicated the excellent properties of PLZT with composition 3/52/48 and reported that the largest value d_{33} x E_{ph} (induced strain) was obtained with this composition.

Poosanaas P. and Uchino K. (1999)[1] reported the latest discovery that. PLZT 4/48/52 and 5/54/46 exhibited both the highest response speed and the highest photo-induced strain. The contour maps for response speed and photo-induced strain are illustrated in Fig.3.4 and 3.5. Therefore, it seems clear that PLZT 3/52/48, 4/48/52 and 5/54/46 are very important and should be further investigated.

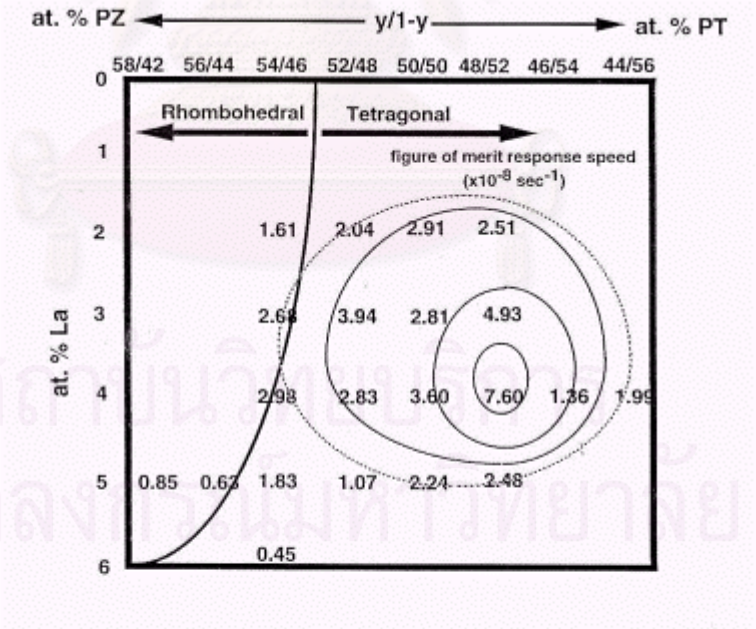

Fig.2.4 The contour map for response speed of PLZT system

PLZT 4/48/52 showed the highest response speed.

[Poosanaas P. and Uchino K. (1999)][1]

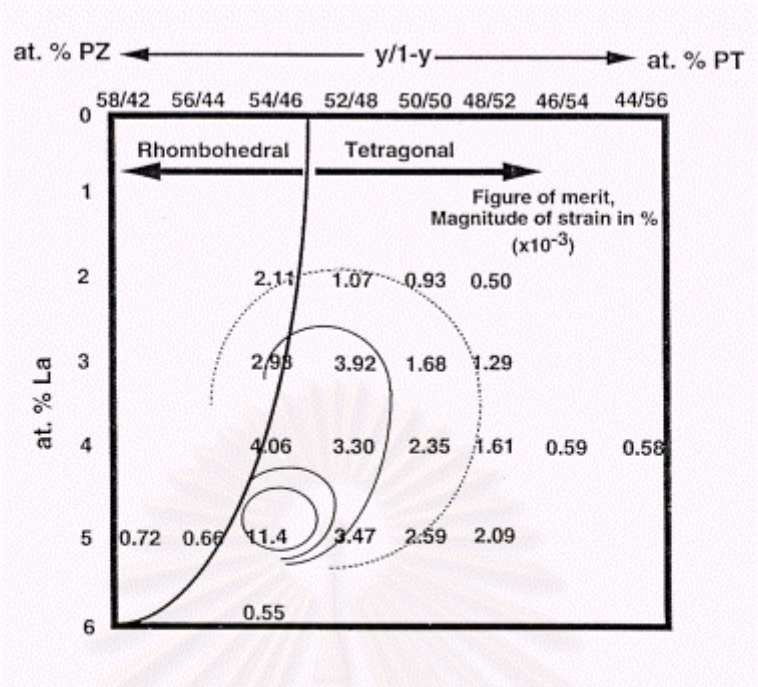

Fig.2.5 The contour map for photo-induced strain of PLZT system PLZT 5/54/46 showed the maximum value. [Poosanaas P. and Uchino K. (1999)][1]

2.4 Effect of dopants on PLZT properties

Dopants can significantly modify the properties of PLZT such as microstructure, electrical and photostrictive properties. These materials are regularly used with a dopant. Doping is commonly employed to improve the properties of basic materials for specific applications. Examples of the frequently used dopants include:

1. Donor additives such as Nb^{5+}, Ta^{5+}, Sb^{5+}, W^{6+} replacing Zr^{4+} or Ti^{4+}.

Since the valences of ions are higher than +4, extra positive charges enter the lattice, Pb vacancies have to be created to ensure electroneutrality.

2. Acceptor additives such as Fe^{3+}, Sc^{3+} or Mg^{2+} replacing Zr^{4+}:

When doping with ions of lower positive valence, oxygen vacancies are created in the lattice, on account of the requirement of electroneutrality.

3. Isovalent additives such as Ba^{2+} or Sr^{2+} replacing Pb^{2+} or Sn^{4+} replacing Zr^{4+}:

The substituting ion has the same valency and approximately the same size as the replaced ion.

Many studies in PZT piezoelectric ceramics reported the positive effect of Nb dopant on their properties. Atkin R.B. and Fulrath R.M. (1971)[13] proposed an increase in the rate of diffusion and densification of PZT by doping five-valent ions such as Nb.

Tanimura M. and Uchino K. (1988)[12] reported the influence of several dopants on the photovoltaic effect in PLZT ceramics as shown in Fig.2.6 and the variation of photo-induced strain with photovoltage for various dopants is illustrated in Fig.2.7. These studies found that the photovoltaic response was enhanced by donor doping onto B-site (Nb^{5+},Ta^{5+},W^{6+}) and concluded that photostriction was proportional to the photovoltaic voltage for materials incorporating dopant ions.

The positive effect of Nb on electrical properties was also found in PZT thin film and was reported by Yuhuan Xu et al. in (1994)[14]. Takao Tani et al. (1997)[15] studied the PZT actuator and pointed out that PZT 55/45 doped with Sr and Nb was a typical material for actuator application. Neurgaonkar et al. (1997)[16] patented the Nb-doped PLZT ceramics and reported that Nb had a great positive effect on dielectric and piezoelectric properties.

Hagimura et al. (1990) and Poosanaas P. (1999)[17] showed that maximum strain, photocurrent and photovoltage could be obtained by doping with rare earth metal such as Gd^{3+}.

From these previous works, it is obvious that the properties of PLZT doped with Nb^{5+} and the promising dopant Gd^{3+} are worth further investigation.

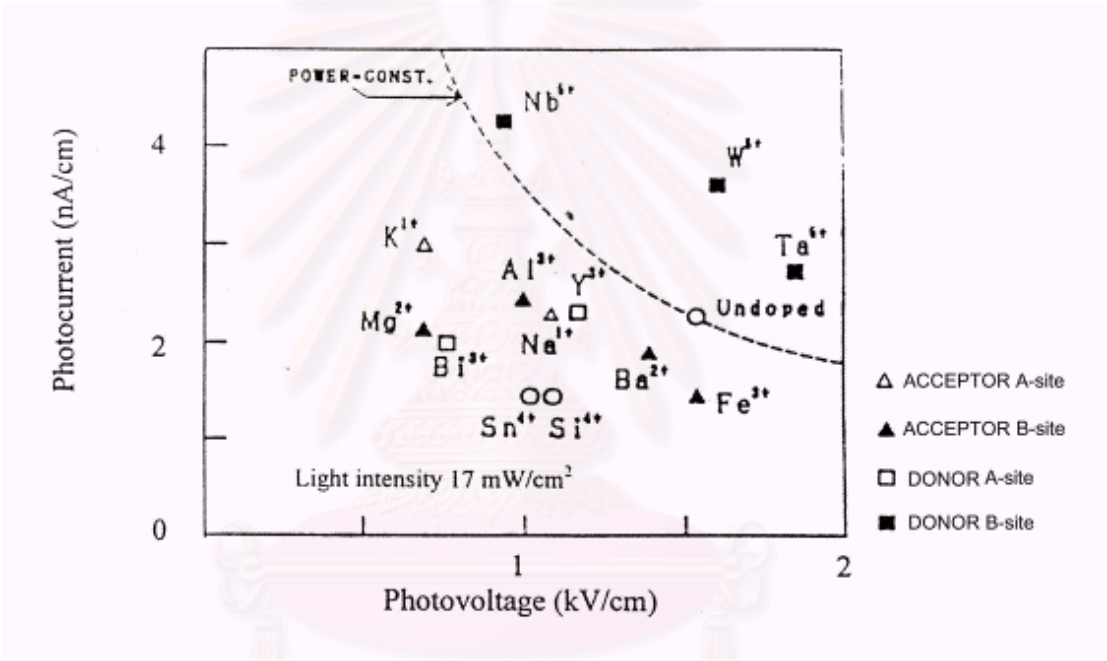

Fig.2.6 Photovoltaic effect with various dopants (1 at% content) in PLZT (3/52/48) ceramics [Tanimura and Uchino (1988)][12]

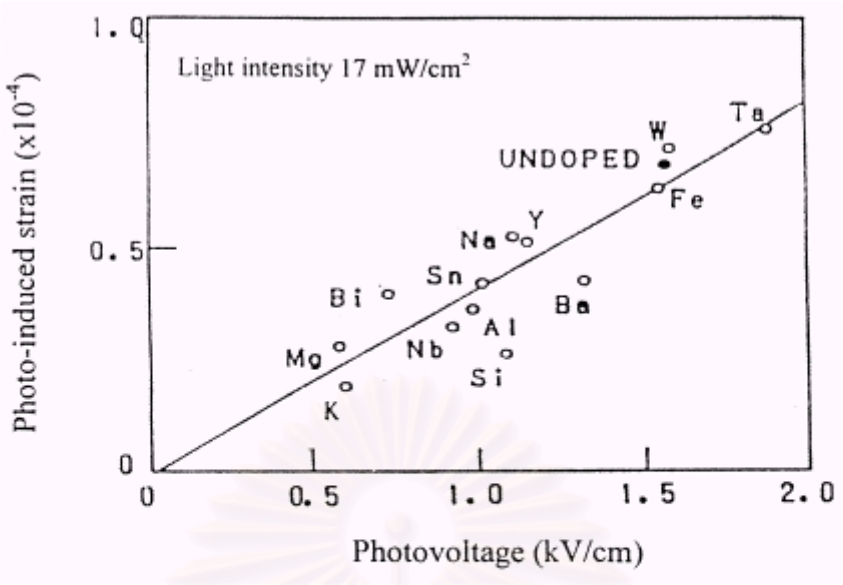

Fig.2.7 Photostriction and photovoltage as a function of various dopants (1 at% content) in PLZT (3/52/48) ceramics [Tanimura and Uchino (1988)][12]

2.5 Effect of grain size on PLZT properties

The photovoltaic and piezoelectric effects are strongly dependent on grain size of the samples. The photovoltaic properties as a function of grain size had been reported by Uchino K. (1997)[11] as shown in Fig.2.8. This study showed the increase in photovoltage with decreasing in grain size and the photocurrent reached the maximum point at a grain size around 2 microns. The photo-induced strain increased with decreasing in grain size while the increasing in piezoelectric constant (d_{33}) was found when increase the grain size. It is obvious that the grain size will affect the piezoelectric and photovoltaic properties of PLZT ceramics.

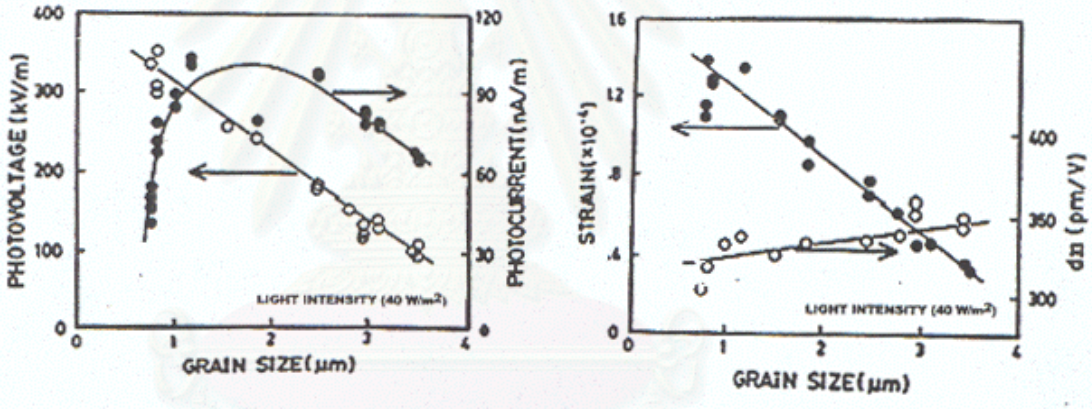

Fig.2.8 Grain size dependence of photostrictive characteristics in PLZT 3/52/48 after Sada et al. (1987) [Uchino K. (1997)][11]

Fig.2.9 shows the experimental results for samples with the composition $Pb_{0.98}(Zr_{0.52}Ti_{0.48})_{0.92}Nb_{0.004}O_3$. In general, piezoelectric properties of ceramics increase approximately with increasing grain size as shown in Fig 2.9 a). This figure showed the increasing in piezoelectric coefficient (d_{33} and d_{31}) with the increasing in grain size. Fig.2.9 b) showed the increasing in the tetragonality with increasing in grain size [Randall, C. A (1998)][21].

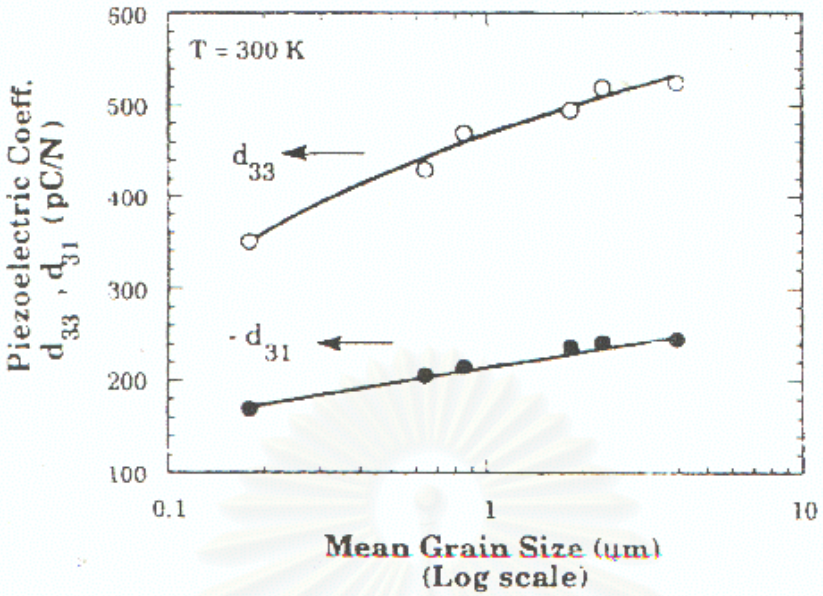

a)

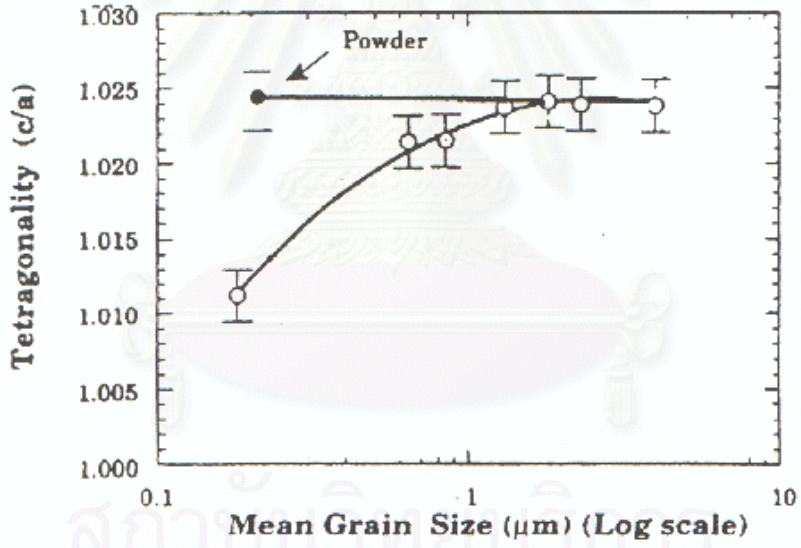

b)

Fig.2.9 Grian size dependence of a) piezoelectric constant b) tetragonality [Randall, C. A (1998)][21]

2.6 Applications based on Photovoltaic and Photostrictive Effects

With decreasing size and weight of actuators the electrical lead wire connecting the actuators to supply electrical power becomes an important limitation for sub-millimeter scale actuators. Therefore, wireless photo-driven actuators activated and driven by incident light, are a very promising candidate for such micro-actuators.

Microactuation and microsensing are two broad classes of the direct conversion from light to mechanical motion applications. The applications for microactuation include [Poosanaas P. (1999)][17]:

- the solar energy converter for converting solar energy directly into mechanical motion for planetary exploration
- the direct corrective controller in adaptive optics/interferometer
- optical micropositioning device
- solar tracking actuator/shutter for self alignment of the spacecraft to the sun
- optically controlled valves for medical or space applications
- optically controlled microrobots

The applications for microsensing include:

- sensors for incident radiation of UV or visible light
- microsensors based on the photodeflection

The photo-driven microactuators can also be used in diverse applications including high precision surgery, minimally invasive medical diagnostics, optical micropositioning, optically controlled microrobots, solar tracking shutter, photostrictive transducers and photophone for the next generation of communication systems.

The application of PLZT wafers photoactuation has been successfully demonstrated as [Uchino K. (1997)] [19]:

- photo-driven relay
- photo-driven micro walking machine

2.7 Examples of Photostrictive and Piezoelectric devices

2.7.1 Photo-acoustic device (Photophone)

Photo-mechanical resonance of a PLZT ceramic bimorph had been successfully induced using chopped near-ultraviolet irradiation, having neither electric lead wires nor electric circuits [Uchino K. (1997)][19]. A thin cover glass was attached on the photostrictive bimorph structure to decrease the resonance frequency so as to easily observe the photo-induced resonance. Fig.2.10 shows the experimental setup with an optical chopper. A dual beam method was used to irradiate the two sides of the bimorph alternately. The mechanical resonance was then determined by changing the chopper frequency.

Photo-induced mechanical resonance was successfully observed. The resonance frequency was about 75 Hz with the mechanical quality factor of about 30. The maximum tip displacement of this photostrictive sample was about 5 μm at the resonance point, smaller than the level required for audible sound. However, the achievement of photo-induced mechanical resonance in the audible frequency range suggests the promise of photostrictive PLZT bimorph type devices as photo-acoustic component, or photophone, for the next optical communication age.

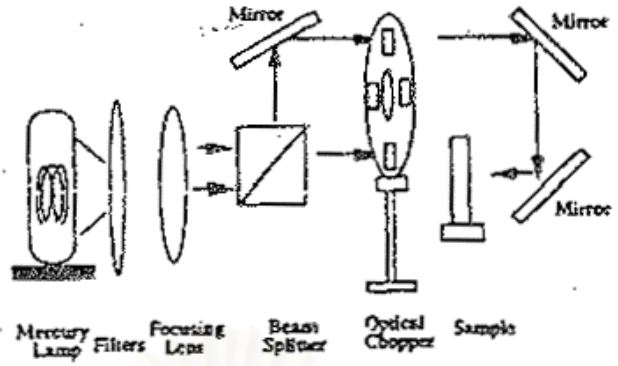

Fig.2.10 Experimental setup for photo-induced mechanical resonance using an optical chopper [Uchino K. (1997)][19]

2.7.2 Piezoelectric buzzer

In the use of mechanical vibration devices such as filters or oscillators, the size and shape of device are very important, and both the vibrational mode and the ceramic material must be considered. The resonance frequency of the bending mode in the centimeter-size sample range from 100 to 1000 Hz, which is much lower than that of the thickness mode (100 kHz). For these vibrator applications the piezoelectric ceramic should have a high mechanical quality factor (Q_M) rather than a large piezoelectric coefficient. That is, hard piezoelectric ceramics are preferable.

For speaker or buzzer, audible by human, devices with a rather low resonance frequency are used (kHz range). Examples are a bimorph consisting of two piezoelectric ceramic plates boned together, and a piezoelectric fork consisting of a piezo-device and a metal fork as shown in

Fig.2.11 [Uchino K. (2000)][20]. This device has merits such as high electric power efficiency, compact size and long life.

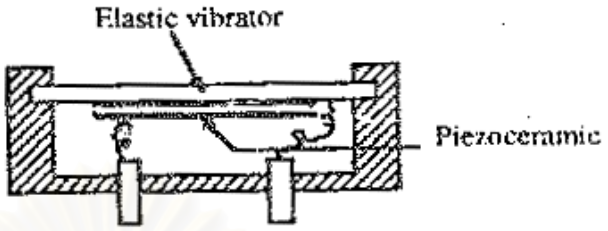

Fig.2.11 Piezoelectric Buzzer [Uchino K. (2000)][20]

2.7.3 Micro walking device

Micro walking device using photoactuating composite films was designed into arch-shape as shown in Fig.2.12 [Poosanaas P.(1999)][17]. These photoactuating composite films may be fabricated from PLZT solutions. The PLZT solutions were coated on one side of a flexible substrate which has a curvature about 1 cm^{-1}. The lengths of the right and the left legs were slightly different to provide a difference between their resonance frequencies. The device could be controlled in both clockwise and counterclockwise rotation. The maximum vibration motion of this device could be obtained by using the light source frequency near the resonance frequency of the bimorph. Under illumination on the upper side of the device, the PLZT film, being bonded onto substrate, would contract and the device would then decrease the curvature and move.

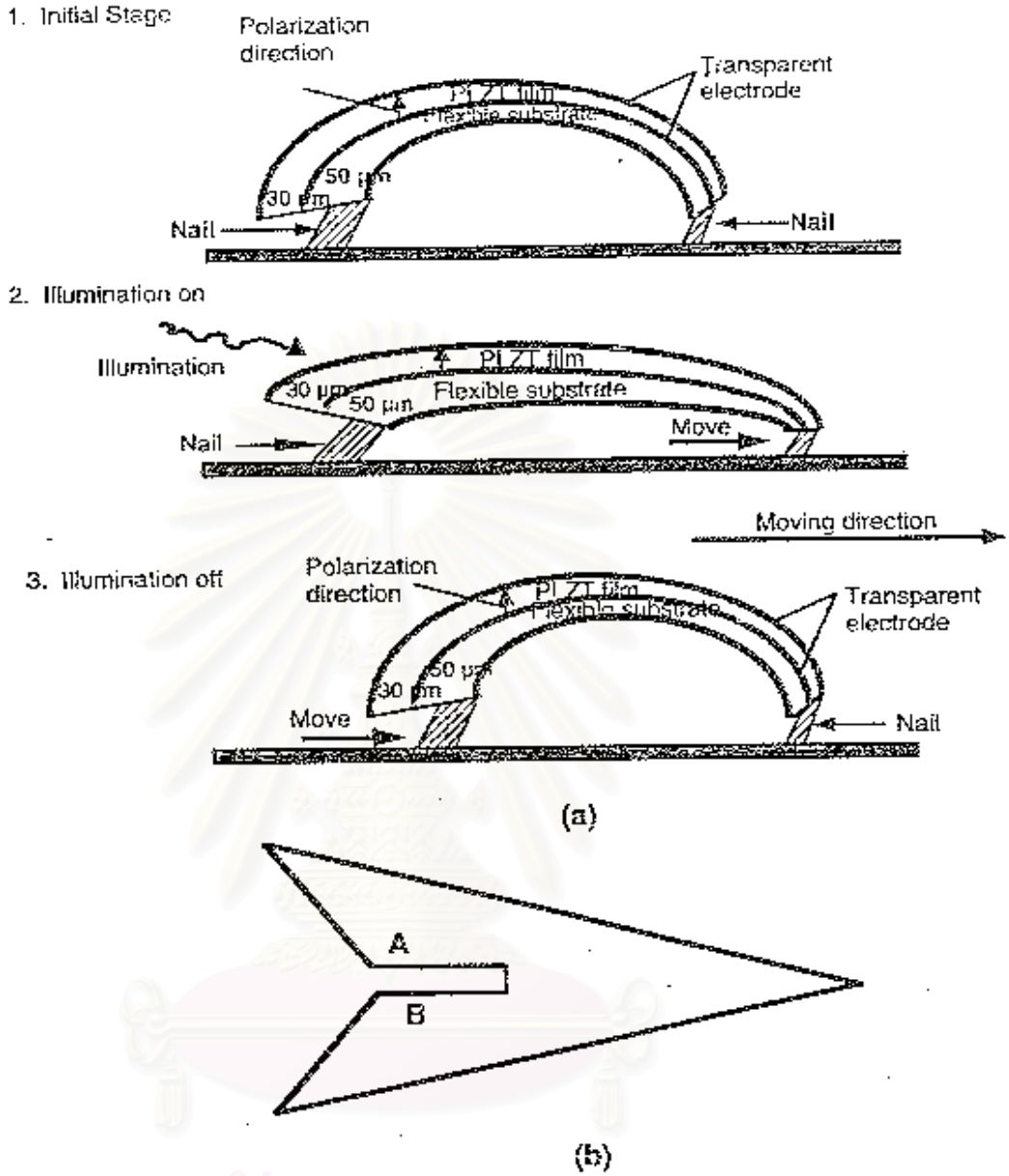

Fig.2.12 a) Arch-shaped type photoactuating film composites
b) the triangular top shape photoactuating film composites
[Poosanaas P.(1999)][17]

2.7.4 The light source chasing device

Photoactuating film composites were used as a light chasing device. Fig.2.13 shows the principle of this device [Poosanaas P.(1999)][17]. Two unimorphs were attached to both sides of a solar panel. The strain of two unimorphs were the key factor. When the light source was positioned at the center between two unimorphs, their strain would equal and result in the stable state of the solar panel. When the light source moved to one side, the intensity of light at that side would be stronger than the other. Hence the photoactuating film on that side would deflect more and lead to a motion towards the light source.

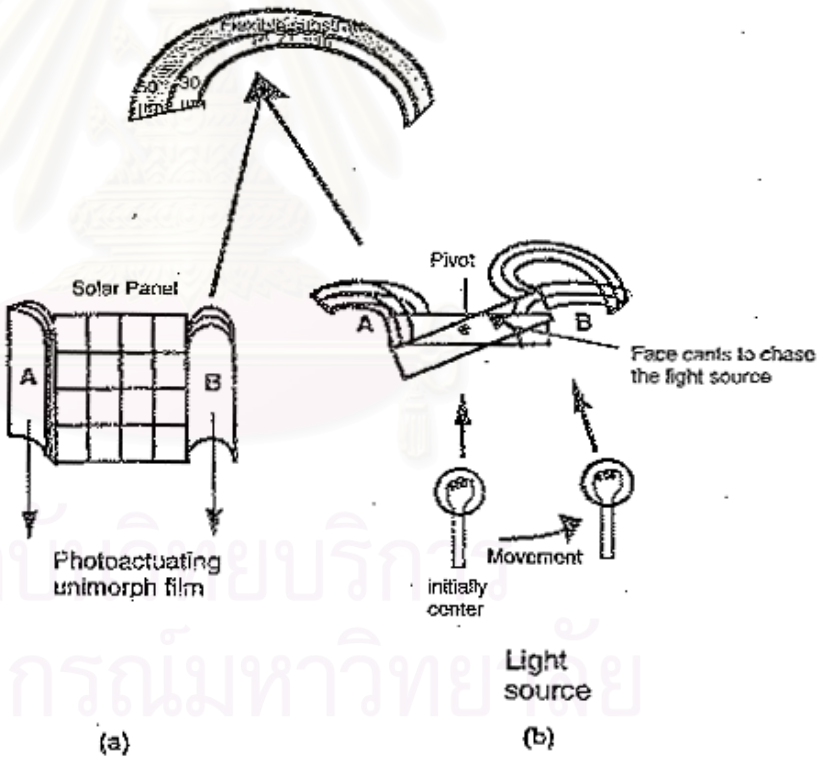

Fig.2.13 a) The light source chasing device based on photoactuating film composites b) schematic diagram of the device movement [Poosanaas P.(1999)][17]

Since photostrictive actuators are driven only by the irradiation of light, They are suitable to use in actuators, in which lead wires can hardly be connected because of their ultra small size or their employed conditions such as ultra-high vacuum or outer space. The new principle actuators have considerable effects upon the future micro-mechatronics.

CHAPTER 3
EXPERIMENTAL WORK

3.1 Preparation of Powders and Polycrystalline samples

PLZT (3/52/48) ceramics doped with 0.5 at% Nb_2O_5 and 0.5 at% Gd_2O_3 were selected due to its high photovoltaic and photostrictive properties [Nonaka K. et al.(1995)][10]. Recently, a rigorous study on the composition dependence of PLZT ceramics on photostrictive properties, shown that the highest response speed and highest photo-induced strain were found at PLZT (4/48/52) and (5/54/46), respectively [Poosanaas P. and Uchino K. (1999)][1]. Therefore, it is worthwhile to study and improve the properties of photostrictive ceramics through the doping effect of PLZT (4/48/52) and (5/54/46) with Nb_2O_5 and Gd_2O_3 dopants. PLZT (4/48/52) and (5/54/46) doped with 0.5 at% Nb_2O_5 and 0.5 at% Gd_2O_3 were also studied for this research.

PLZT powders were prepared by a conventional oxide mixing process with reagent grade lead oxide (PbO), lanthanum oxide (la_2O_3), zirconium oxide (ZrO_2), titanium oxide (TiO_2) and dopants. The chemical purity and suppliers are listed in Table 3.1 and the conventional oxide mixing flow chart is illustrated in Fig.3.1.

In this method, the raw materials were weighed and mixed in the proper ratio to attain the required composition and ball milled in water for 10 hours. The slurry was dried at 110°C and then calcined at 950°C for 10 hours in a closed alumina crucible. The calcined powders were further ball milled for 10 hours and then mixed with 1 wt% PVA binder (molecular weight 15,000). The powders were then pressed into pellets using a pressure of 80 MPa. The pellets were heated at 540°C for binder burn out and subsequently sintered at 1250°C for 2 hours in a PbO atmosphere. The calcination and sintering steps

are illustrated in Fig.3.2 and Fig.3.3, respectively.

Table 3.1 Component oxide powders used in the synthesis of PLZT ceramics by conventional oxide mixing process

Materials	Grade	Manufacturer
Lead oxide (PbO)	99.0 %	Fluka
Lanthanum oxide (La_2O_3)	99.98 %	Fluka
Zirconium oxide (ZrO_2)	~3% HfO_2	Fluka
Titanium oxide (TiO_2)	99.5 %	Unilab
Niobium oxide (Nb_2O_5)	>99.95 %	Kanto Chemical
Gadolinium oxide (Gd_2O_3)	99.9 %	Aldrich

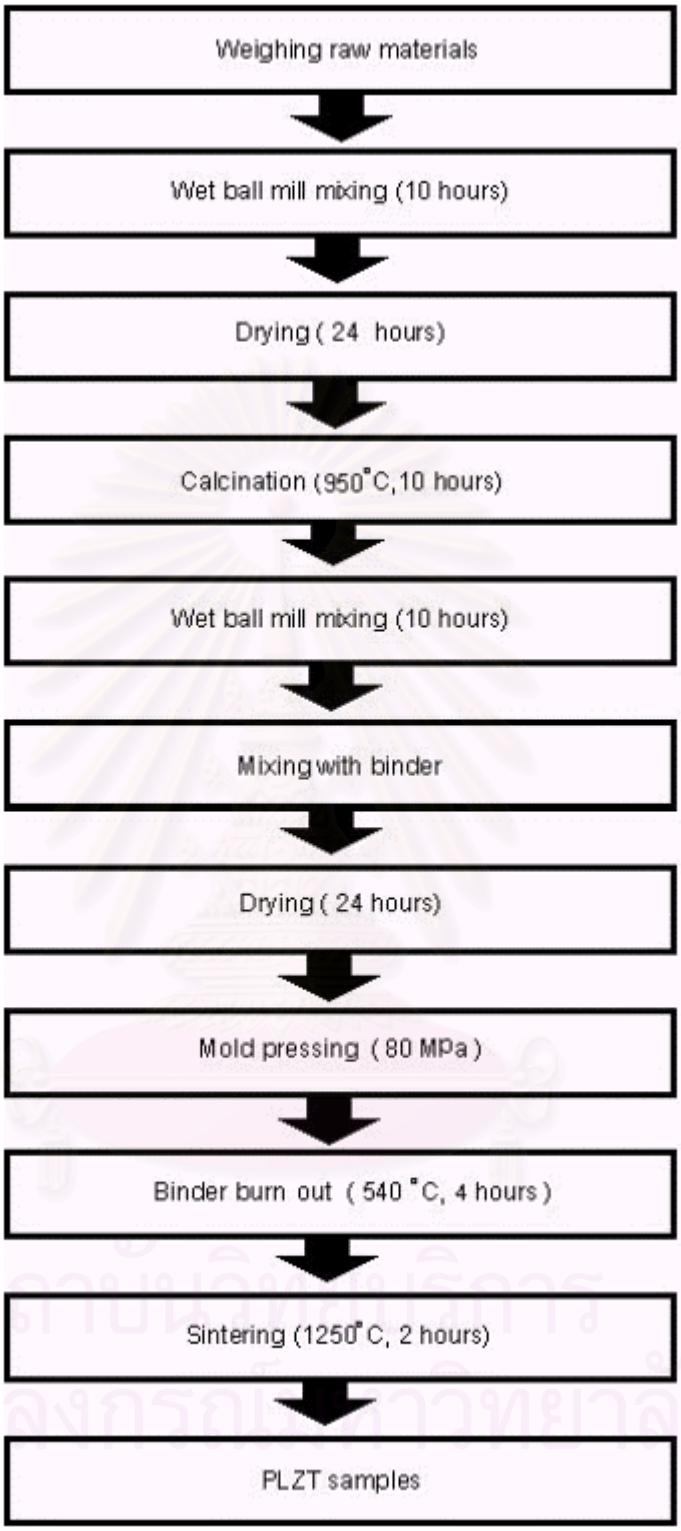

Fig.3.1 The conventional oxide mixing flow chart of PLZT ceramics

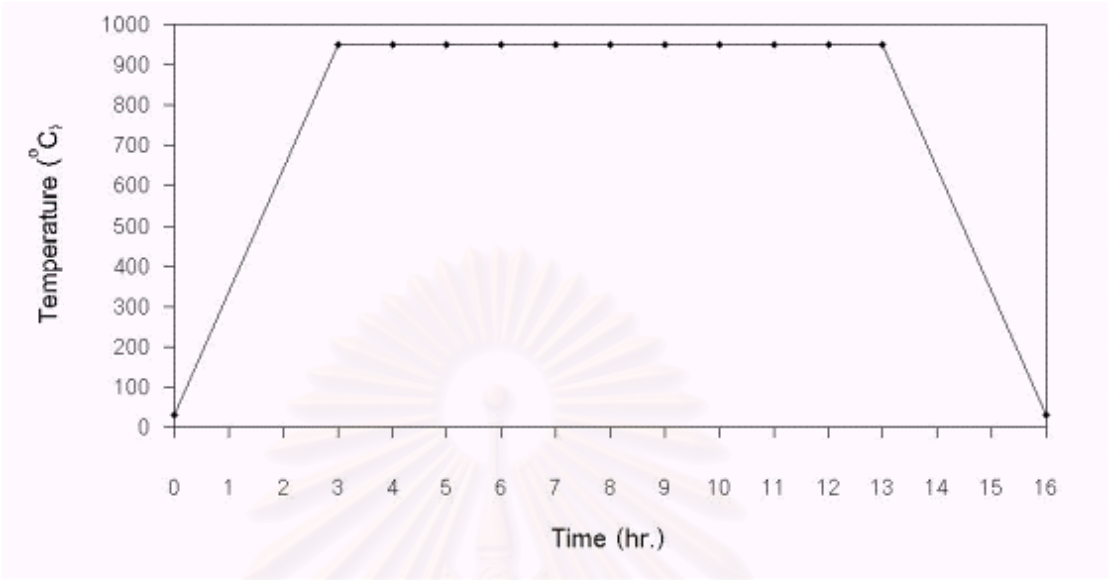

Fig.3.2 The calcination step for preparation of PLZT ceramics

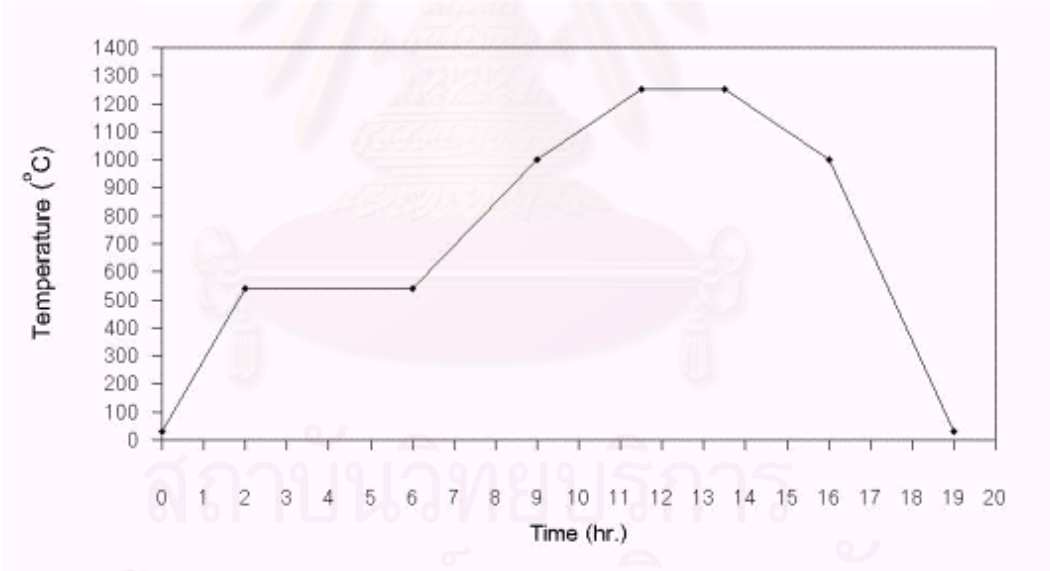

Fig.3.3 The sintering step for preparation of PLZT ceramics

3.2 Characterization of Ceramic Specimens

3.2.1 Phase Analysis of PLZT powders

X-ray diffraction (XRD) was used to identify phases present in the calcined powders and the sintered samples. An X-ray diffractometer (Jeol, JDX 3530) was employed under CuKα radiation (λ = 1.5418 Å) scaning angle, 2θ, 20°- 90°, using 0.04 degree step angle and 0.5 second count time.

3.2.2 Microstructure Analysis

Microstructure characteristics of sintered PLZT samples, such as grain size and shape, were characterized using Scanning Electron Microscope (Jeol, JSM 5410). The sintered samples were polished down to 1 micron and then thermally etched at 1100 °C for 10 min. The etching temperature was kept lower than the sintering temperature in order to prevent the grain growth. The surfaces of polished samples were gold-coated for 90 seconds to reduce the charging during SEM operation. The average grain size was determined by the line intercept method.

3.2.3 Bulk Density and Relative Density of Sintered Samples

Bulk Density, and relative density of the sintered samples were determined by the Archimedes method (ASTM standard Designation: c 20-00). In the beginning, the specimens were dried by heating at 105 to 110°C and the dry weight approximately of 0.1 g, D, was accurately determined. The test specimens were then placed in water and boiled for 2 hours. The specimens were kept entirely under the water during the boiling period without

the contact with the bottom of the container. After being immersed in the water for at least 12 hours, the suspended weight, S, of the specimens was determined by suspending the specimen in a loop of copper wire hung from the arm of the balance. After that, each specimen was wiped lightly with a moistened smooth linen or cotton cloth to remove the water drops from the surface in order to determine the saturated weight, W, in air.

The following equations were used to calculated bulk density.

$$\text{Exterior volume, (V)} = W-S$$

$$\text{Bulk density (B) g/cm}^3 = D/V$$

Theoretical density of the PLZT sample can be obtained from the molecular weight of PLZT, which taken from the weight of all the atoms in one tetragonal unit cell, and the volume of the tetragonal unit cell. Lattice parameters of the unit cell were determined from the two characteristic X-ray peaks (hkl), (200) and (002). The theoretical density was calculated from the relation as follows.

$$\text{Theoretical density} = \frac{m_{PLZT}}{V_{unit}}$$

Where m_{PLZT} is the molecular weight (g) of the PLZT in one unit cell and V_{unit} is the volume of the tetragonal unit cell (cm^3)

The relative density of PLZT sample was then calculated from

$$\text{The relative density} = \frac{\text{Bulk density}}{\text{Theoretical density}} \times 100$$

3.2.4 Dielectric and Piezoelectric properties

3.2.4.1 Dielectric properties

The dielectric constant (K) was determined for PLZT samples. They were polished to about 10 mm in diameter and 1 mm in thickness and then electroded with silver paste on both sides. The electroded samples were poled in silicone oil at 120°C under 2 kv/mm electric field for 15 min. The capacitance (C) and the dissipation factor of the samples were measured by Impedance Analyzer (Hewlett Packard 4192A LF). The dielectric constant was calculated from this capacitance value from the following equation [Buchanan R.C. (1991)][4].

$$K = \frac{Ct}{\varepsilon_0 A}$$

where C is the capacitance (Farad), ε_0 is the permitivity of free space (8.854×10^{-12} F/m), A and t are the electroded area (m^2) and thickness (m) respectively.

3.2.4.2 Pizoelectric properties

The samples with the same dimensions as the ones for dielectric measurements were poled in silicone oil at 120°C under 2 kV/mm electric field for 15 min, and their piezoelectric properties were measured with a Piezo d-meter (Berlincourt model CADT) at 120 Hz.

3.2.5 Photovoltage and Photocurrent Measurement

The samples were polished down to 1 micron and 1 mm in thickness.

These samples were cut to a size of 3 mm x 6 mm x 1 mm, electroded with silver paste on both 6 x 1 mm^2 surfaces and then poled in silicone oil at 120^{o}C under 2 kV/mm electric field for 15 min.

Photovoltage and Photocurrent were measured by applying voltage between –100 and +100 V, and detecting the current (electrometer Keithley 617) while illuminating the sample. The schematic diagram for Photovoltage and Photocurrent measuring system is illustrated in Fig.3.4.

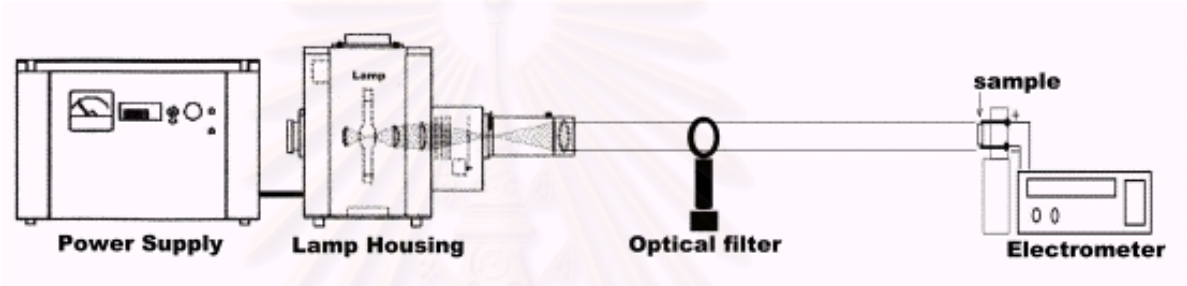

Fig.3.4 The schematic diagram for Photovoltage and Photocurrent measuring system

A super-high pressure, short arc mercury lamp (Ushio USH-500SC), installed in lamp housing (Ushio SX-UI500HQ), was used as a light source. The radiation from this mercury lamp was passed through an infrared-cut optical filter (Newport 10SWF-500) to cut the wavelength above 500 nm. The light beam generating maximum photovoltaic effect was then applied to the PLZT sample.

The data were plotted using the applied voltage and the measured current as horizontal and vertical axes, respectively. The photovoltage was determined from the intercept of the horizontal applied voltage axis while the photocurrent was determined from the intercept of the vertical measured current axis as shown in Fig.3.5 [Tanimura M. and Uchino K.(1988)][12].

Measurements were made after the samples were thermally equilibrated with the radiation.

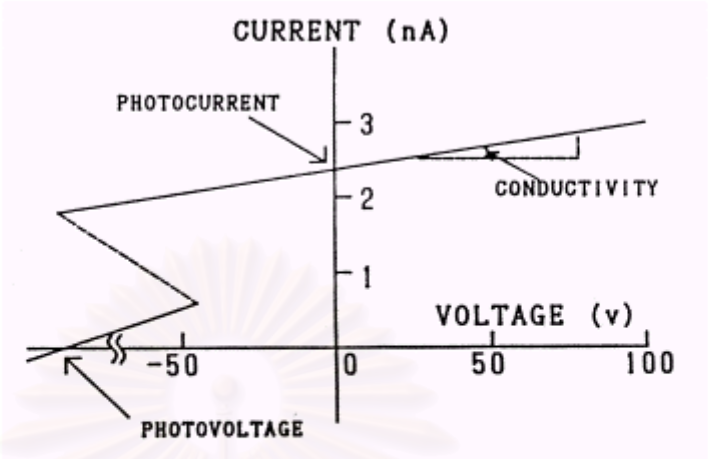

Fig.3.5 Photocurrent measured as a function of applied voltage [Tanimura M. and Uchino K.(1988)][12]

3.3 Fabrication of Photostrictive devices

The sintered samples were cut into 3 mm x 6 mm x 1 mm, the same dimensions as the ones for photovoltage and photocurrent measurements. These samples were electroded and poled in silicone oil at 120oC under 2 kV/mm electric field for 15 min and then connected together to fabricate the devices – photocurrent power supply and micro walking. The photovoltage and the photocurrent of these two devices were measured by applying voltage between –100 and +100 V and detecting the current (electrometer Keithley 617) while illuminating the devices. Design of devices would be explained in Chapter 4.

CHAPTER 4
RESULTS AND DISCUSSION

4.1 Phase analysis of PLZT samples

X-ray diffraction (XRD) pattern was used to identify phases presented in calcined powders and sintered samples using X-ray diffractometer scanning through 20^{o}- 70^{o}. PLZT powders were calcined at different temperatures for 10 hours in order to select the calcining temperature by investigating the forming of a tetragonal phase. XRD patterns of PLZT powders at different calcining temperatures are illustrated in Fig.4.1. XRD patterns of undoped and doped PLZT samples of compositions (3/52/48), (4/48/52), and (5/54/46) ,sintered at 1250^{o}C for 2 hours are shown in Fig.4.2–4.4, respectively.

PLZT powder calcined at 850^{o}C showed the mixed phases of $PbZrO_3$ and $PbTiO_3$ while the single phase of PLZT was observed at 900^{o}C. However, the complete crystallization of the tetragonal phase occurred at higher calcining temperature about 950^{o}C, so this temperature was taken as the experimental condition for calcining. This result also agreed well with previous study which reported the calcining temperature at 950^{o}C [Tanimura M. et al. (1988), Poosanaas P. (1999)][13,18]

XRD patterns of sintered, undoped and 0.5 at% Gd_2O_3 and Nb_2O_5 doped PLZT (3/52/48), (4/48/52), and (5/54/46) ceramics showed the similar results of X-ray diffraction patterns (Fig.4.2-.4.4). In these figures, the reflections from (111) and (200) planes were chosen for phase analysis. The split of (200) peak into two peaks, (200) and (002), indicated the characteristic of the tetragonal phase which has unequal lattice parameters (c > a).

In addition, the XRD patterns of all the sintered samples presented in this study showed the single (111) peak, which is another characteristic of the

tetragonal phase. This confirmed that PLZT samples of all compositions and dopants formed the tetragonal phase which was crucial for ferroelectrics.

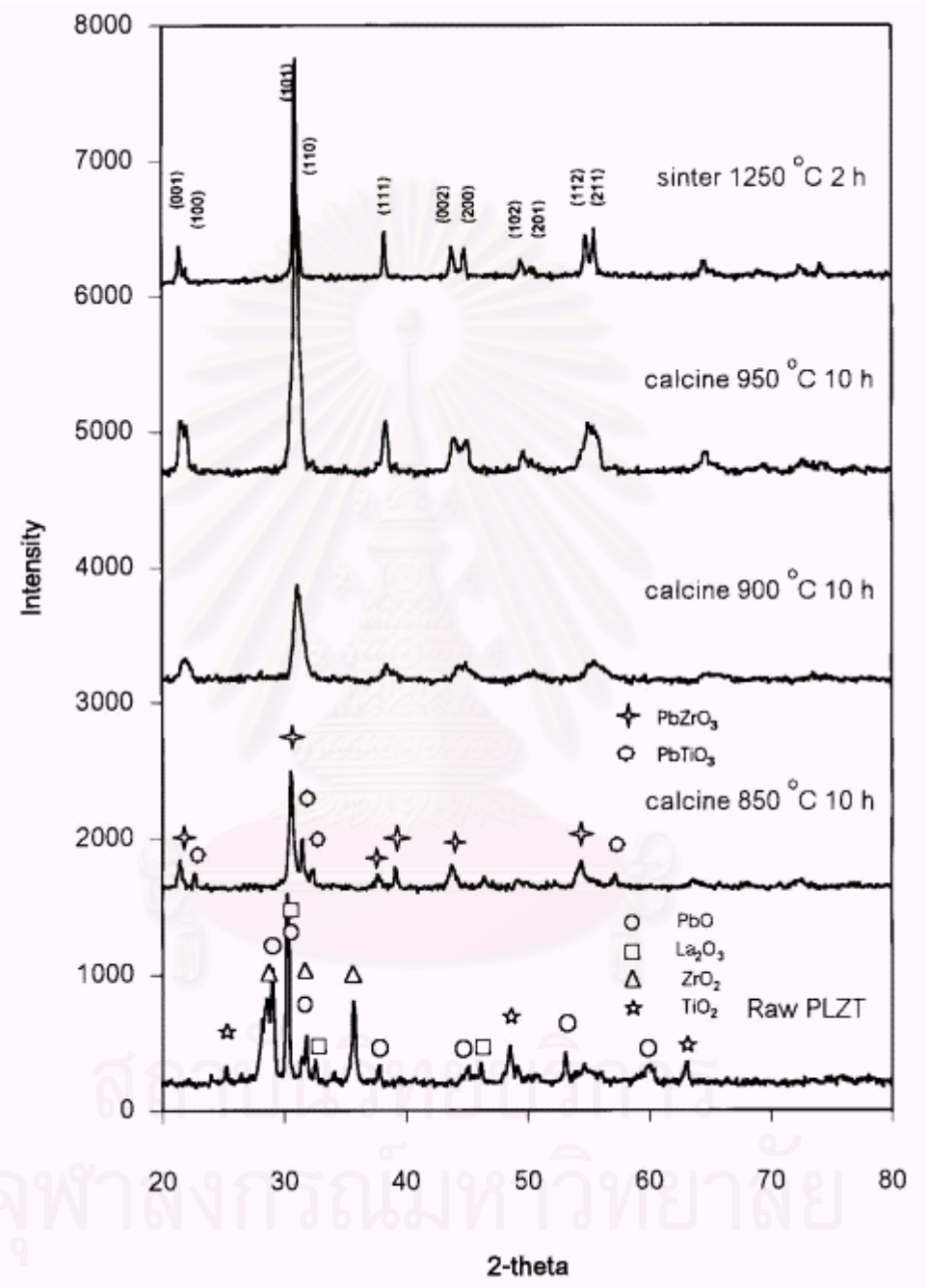

Fig.4.1 XRD patterns of PLZT (3/52/48) powder and sintered ceramics calcined at different temperatures

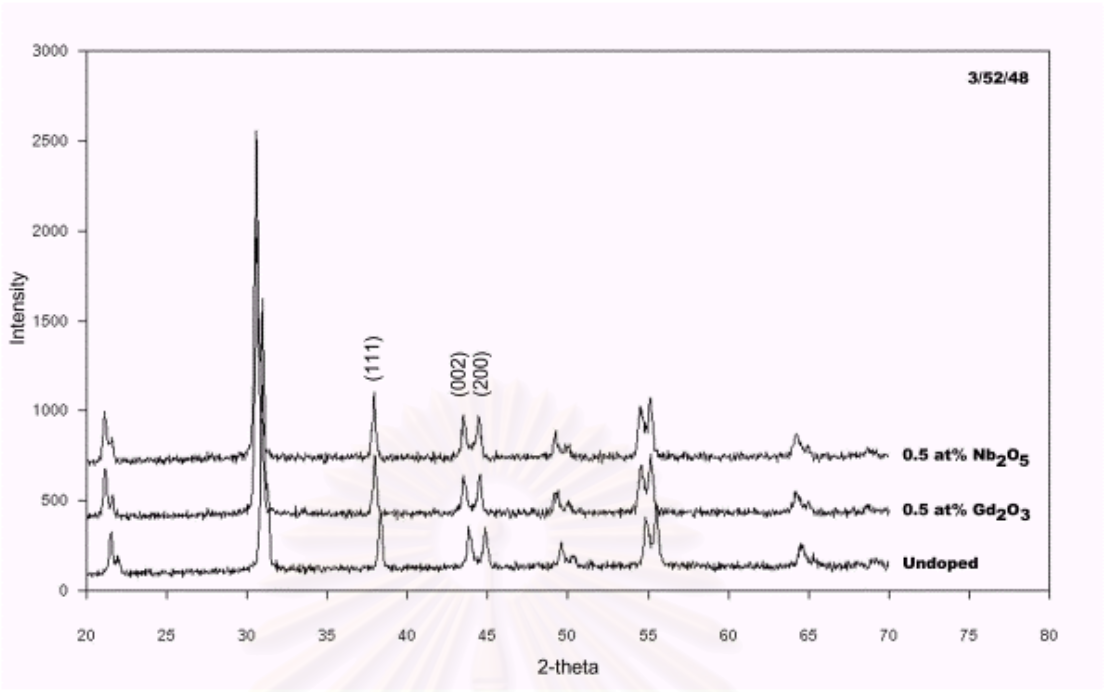

Fig.4.2 XRD patterns of undoped and doped PLZT 3/52/48 ceramics

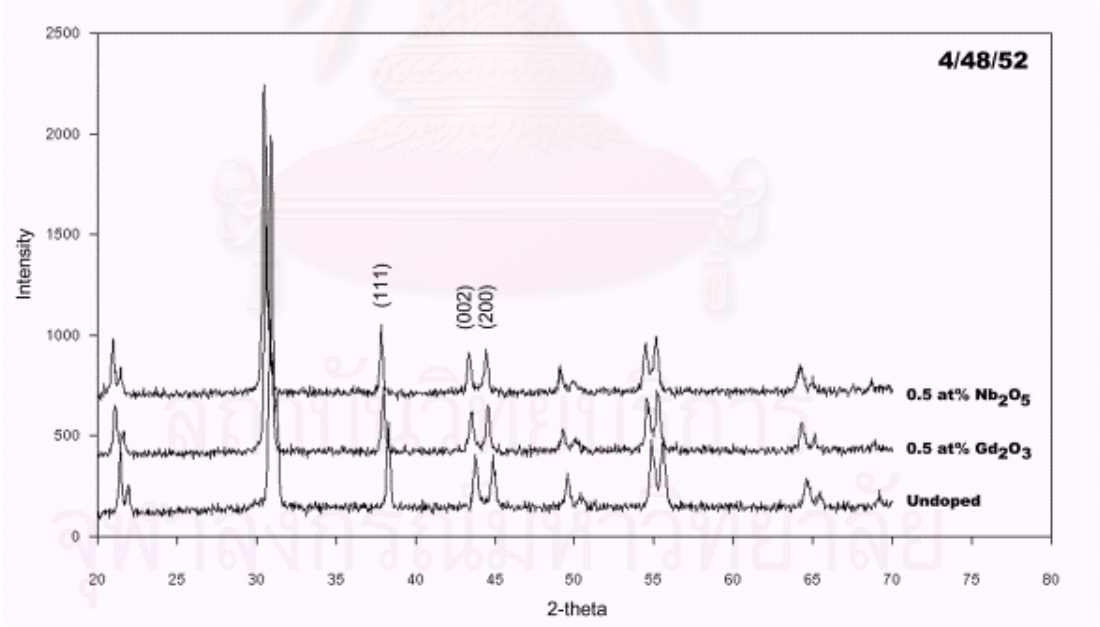

Fig.4.3 XRD patterns of undoped and doped PLZT 4/48/52 ceramics.

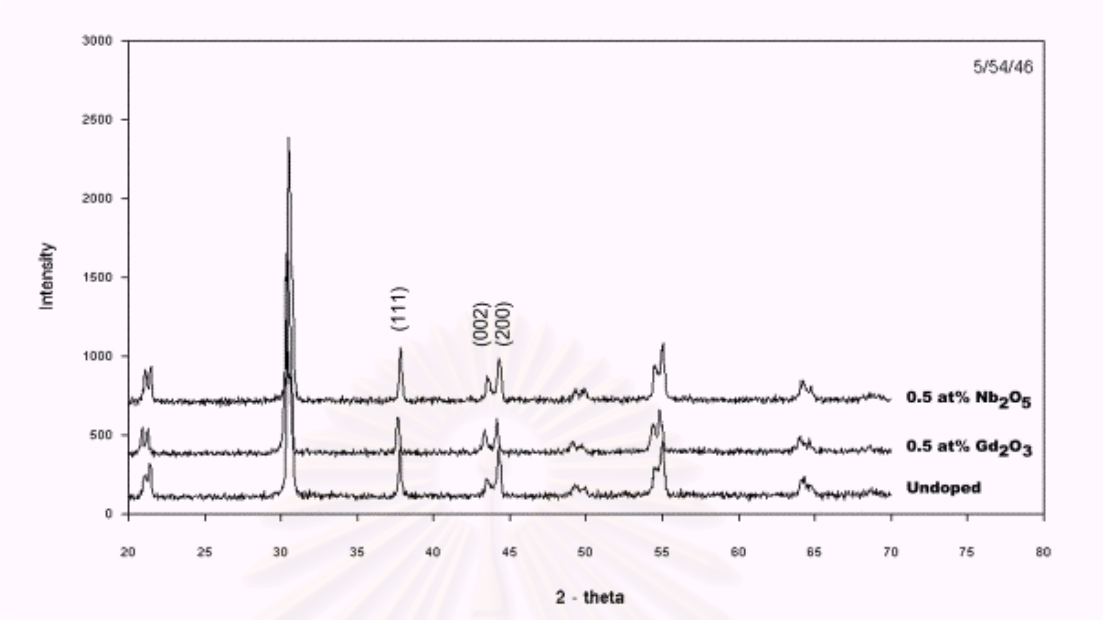

Fig.4.4 XRD patterns of undoped and doped PLZT 5/54/46 ceramics

The effect of dopants on the lattice parameters and the tetragonality (c/a ratio) of PLZT samples can be observed in XRD patterns. The unit cell volume, tetragonality, and lattice parameters of PLZT ceramics were calculated from the XRD peaks. It was found that Gd_2O_3 and Nb_2O_5 increased the unit cell volume of PLZT samples. The lattice parameters and the tetragonality are listed in Table 4.1.

As shown in Table 4.1, lattice parameters of PLZT samples are slightly increased with the dopants (Nb_2O_5 and Gd_2O_3). The tetragonality was only slightly different between each composition but the effect of dopants on the tetragonality was not seen in these results. PLZT 4/48/52 ceramics showed the highest tetragonality while the smallest values presented in PLZT 5/54/46 ceramics.

Table 4.1 Lattice parameters, tetragonality, and unit cell volume of the sintered PLZT samples (calculated from the XRD patterns)

Compositions	Dopants	c (Å)	a (Å)	c/a	Unit cell volume ($x10^{-23}cm^3$)
3/52/48	Undoped	4.1303	4.0427	1.0217	6.7503
	Gd_2O_3	4.1592	4.0703	1.0218	6.8907
	Nb_2O_5	4.1592	4.0703	1.0218	6.8907
4/48/52	Undoped	4.1339	4.0359	1.0243	6.7335
	Gd_2O_3	4.1592	4.0634	1.0236	6.8673
	Nb_2O_5	4.1702	4.0738	1.0237	6.9208
5/54/46	Undoped	4.1592	4.0878	1.0175	6.9501
	Gd_2O_3	4.1739	4.1019	1.0176	7.0228
	Nb_2O_5	4.1592	4.0878	1.0175	6.9501

This result could be explained by considering the PLZT contour map, which showed the region between tetragonal and rhombohedral phases. PLZT 4/48/52 displayed the highest tetragonality because its location in the tetragonal region was far away from phase boundary while that of PLZT 5/54/46 located closer to the phase boundary as shown in Fig.4.5. However, the XRD patterns of PLZT (3/52/48) and PLZT (4/48/52) showed the small amount of rhombohedral phase. This could be observed from the intensity of (002) and (200) peaks which had no significant deference. Unlike PLZT (3/52/48) and PLZT (4/48/52), PLZT (5/54/46) showed the higher intensity of (200) peak, which indicated that this composition showed the complete tetragonal phase.

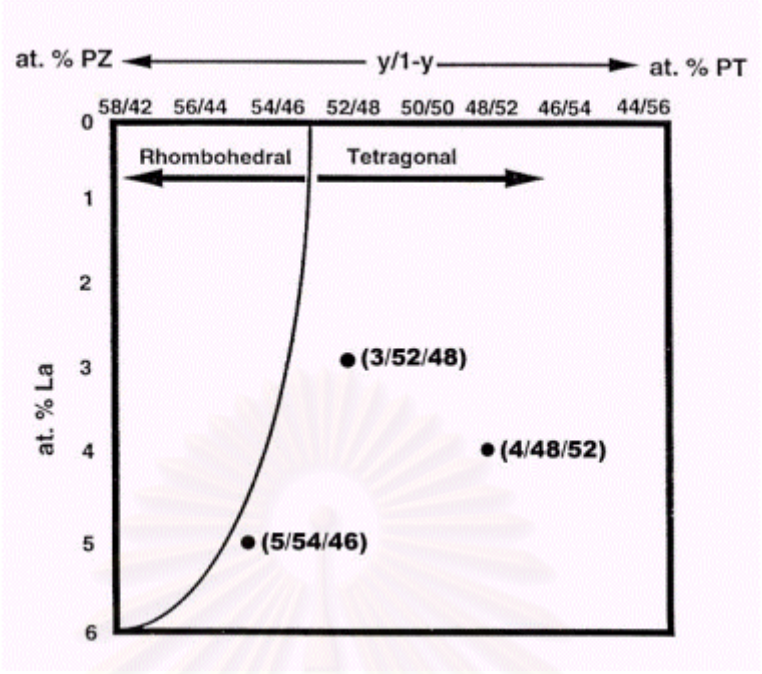

Fig.4.5 PLZT compositional contour map

4.2 Microstructure Analysis

SEM micrographs of thermally etched PLZT samples are shown in Fig.4.5-4.13. The average grain sizes determined by the intercept method are listed in Table 4.2.

It was found that the average grain size was different for each composition of PLZT ceramics. The smallest grain was presented in PLZT 4/48/52 while it showed the largest grain size in PLZT 3/52/48. The average grain size of each composition had the same tendency. Grain size of PLZT samples increased with Nb_2O_5 and Gd_2O_3 dopants. Gd_2O_3 was found to increase grain size of PLZT ceramics more than Nb_2O_5. The effect of composition and type of dopants on the average grain size is summarized in Fig 4.6.

Table 4.2 The average grain sizes of PLZT samples depending on composition and type of dopants

Compositions	Dopants (0.5 at%)	Average grain sizes (micron)
3/52/48	Undoped	1.21
	Gd_2O_3	1.44
	Nb_2O_5	1.36
4/48/52	Undoped	0.83
	Gd_2O_3	1.14
	Nb_2O_5	1.02
5/54/46	Undoped	1.07
	Gd_2O_3	1.31
	Nb_2O_5	1.09

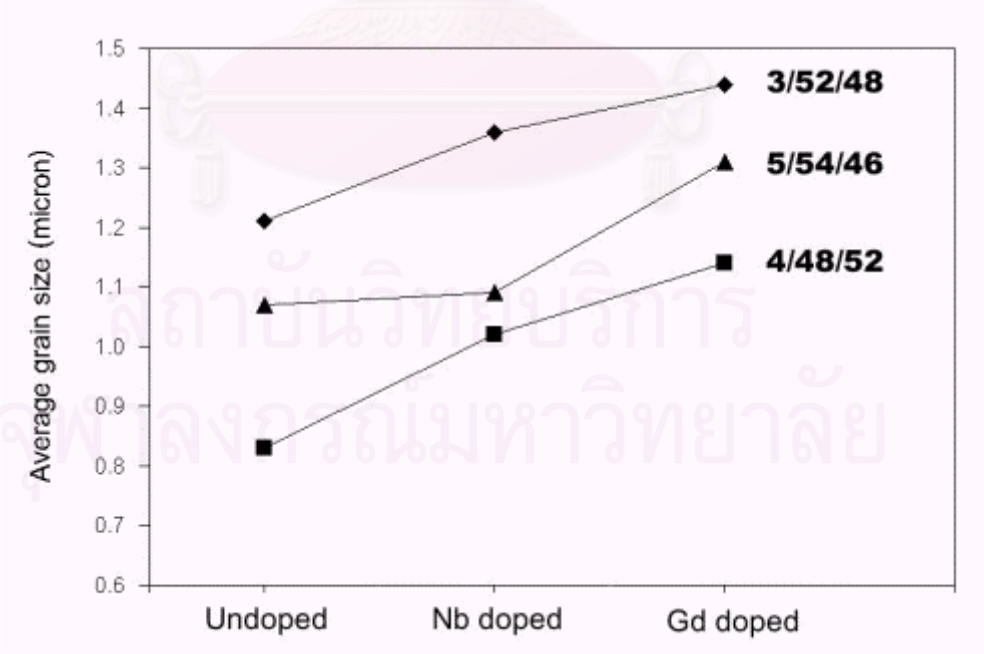

Fig.4.6 The effect of composition and dopants on the average grain size

The SEM micrographs of PLZT samples (Fig.4.5-4.13) showed some entrapped porosity. Microstructures were found to be completely lacked of a second phase, which often precipitated along the grain boundaries or at triple points between grain.

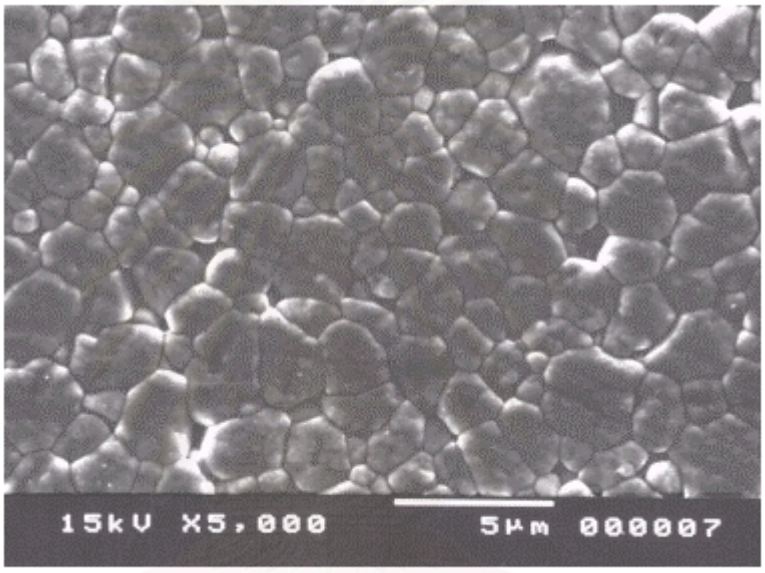

Fig.4.7 SEM micrograph of undoped PLZT 3/52/48 ceramic

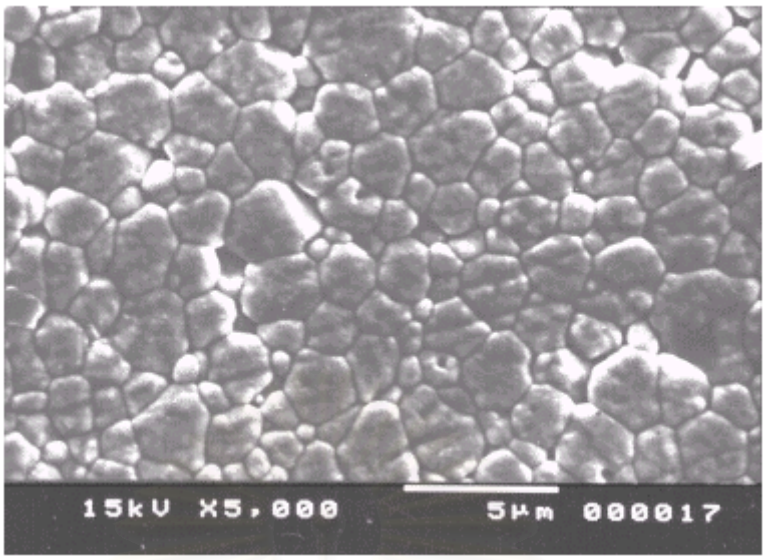

Fig.4.8 SEM micrograph of 0.5 at% Gd_2O_3 doped PLZT 3/52/48 ceramic

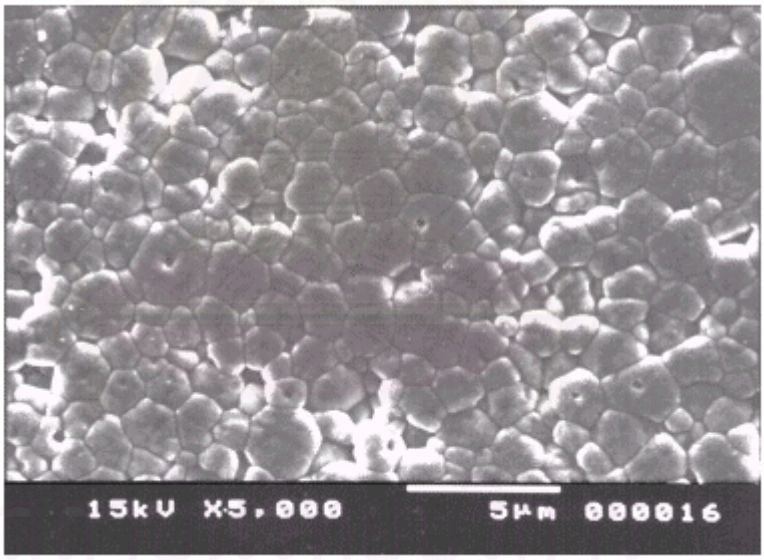

Fig.4.9 SEM micrograph of 0.5 at% Nb_2O_5 doped PLZT 3/52/48 ceramic

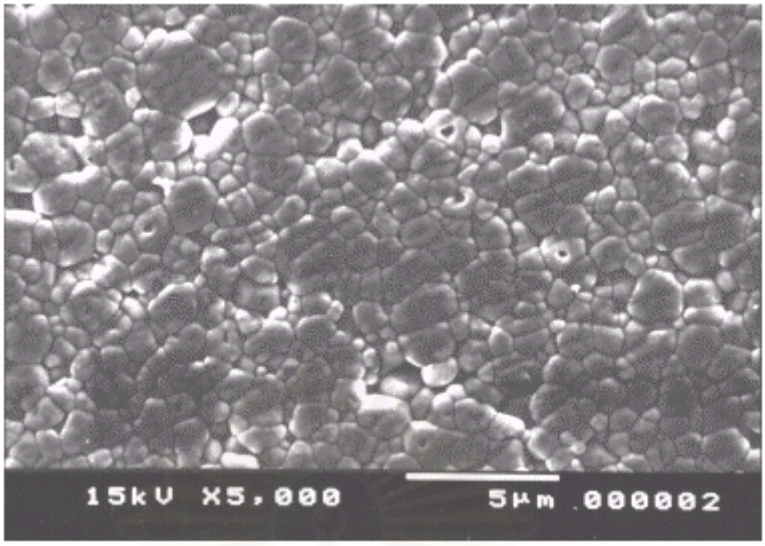

Fig.4.10 SEM micrograph of undoped PLZT 4/48/52 ceramic

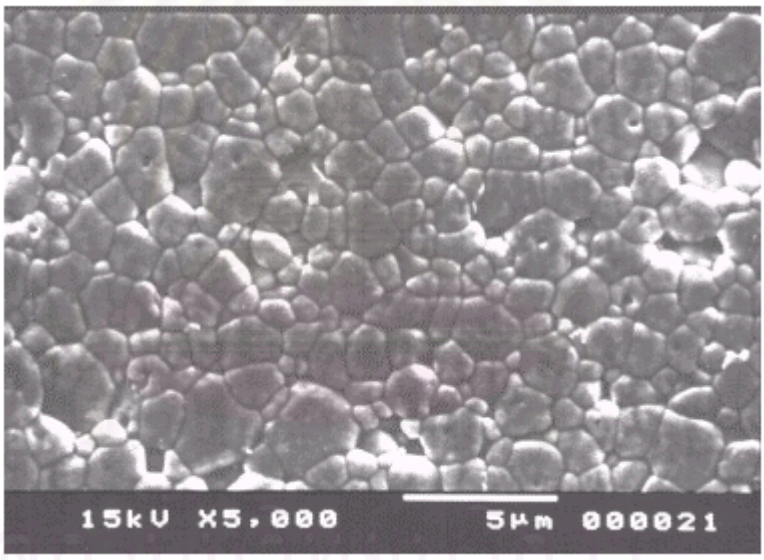

Fig.4.11 SEM micrograph of 0.5 at% Gd_2O_3 doped PLZT 4/48/52 ceramic

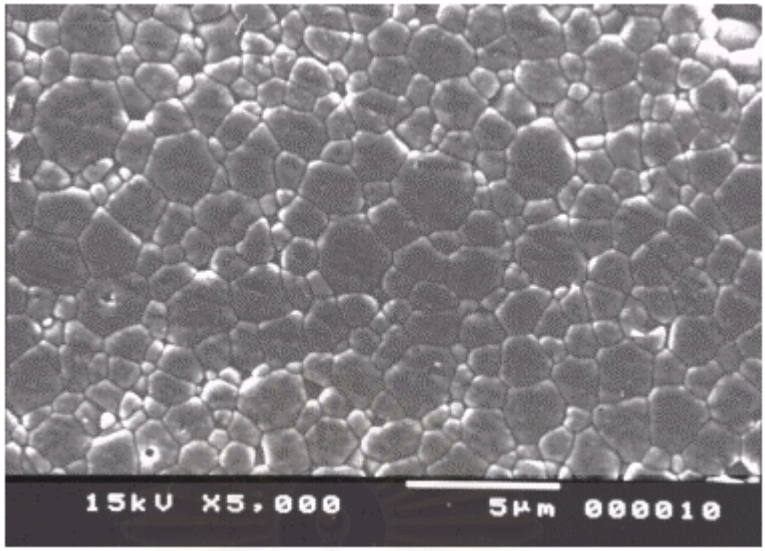

Fig.4.12 SEM micrograph of 0.5 at% Nb_2O_5 doped PLZT 4/48/52 ceramic

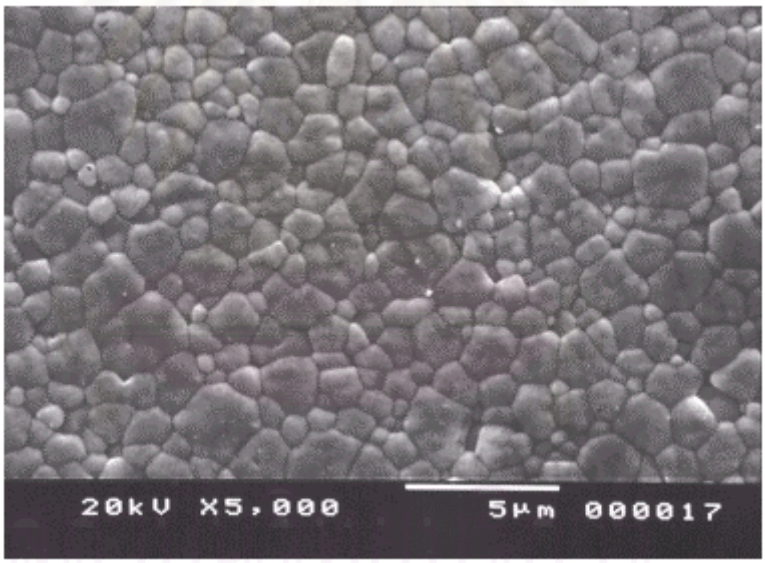

Fig.4.13 SEM micrograph of undoped PLZT 5/54/46 ceramic

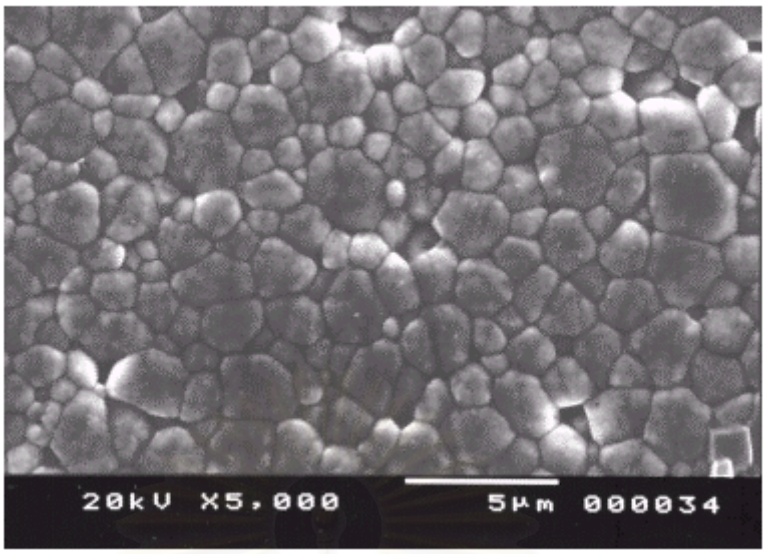

Fig.4.14 SEM micrograph of 0.5 at% Gd_2O_3 doped PLZT 5/54/46 ceramic

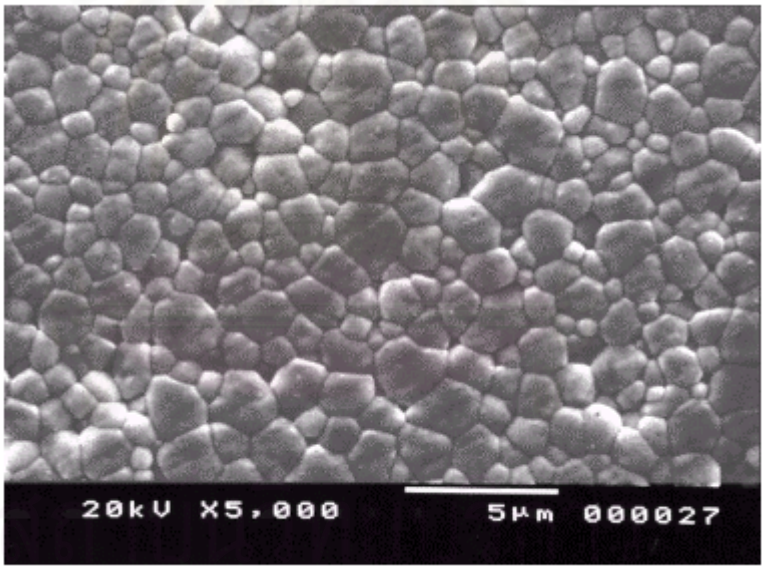

Fig.4.15 SEM micrograph of 0.5 at% Nb_2O_5 doped PLZT 5/54/46 ceramic

4.3 Bulk Density, and Relative Density of sintered samples

Bulk density and relative density of sintered PLZT samples were determined by the Archimedes method (ASTM standard Designation: c 20-00). The results are listed in Table 4.3.

Table 4.3 Bulk density and relative density of sintered PLZT samples

Composition	Dopants (0.5 at%)	Bulk Density (g/cm^3)	Relative density (%)
3/52/48	Undoped	7.86	98.16
	Gd_2O_3	7.72	99.16
	Nb_2O_5	7.70	99.15
4/48/52	Undoped	7.69	97.51
	Gd_2O_3	7.58	97.78
	Nb_2O_5	7.54	98.05
5/54/46	Undoped	7.69	99.87
	Gd_2O_3	7.56	99.20
	Nb_2O_5	7.69	99.46

As shown in Table 4.3, bulk density of sintered PLZT samples were mainly depended on composition. PLZT 3/52/48 ceramics exhibited the highest bulk density while the lowest density was found at PLZT 4/48/52 ceramics. This result agreed with a previous study [Haertling G.H. and Land C.E. (1971)][(2)] in which bulk density decreased linearly with increasing La content. Dopants were found to have only a small effect on bulk density of PLZT ceramics. There is no significant different between the densities of undoped and doped samples.

4.4 Dielectric and Piezoelectric properties

4.4.1 Dielectric properties

The capacitance (C) and the dissipation factor of all the samples were measured by an Impedance Analyzer (Hewlett Packard 4192A LF) at a frequency of 100 Hz. Room temperature dielectric constants of poled PLZT ceramics were calculated from the capacitance values and listed in Table 4.4. Nb_2O_5 dopant was found to increase dielectric constant in PLZT ceramics in all compositions. Among the three undoped compositions, PLZT 5/54/46 showed the highest dielectric constant, and it became maximum with Nb_2O_5 doping.

Table 4.4 Room temperature dielectric constant and the dissipation factor of the PLZT samples (determined at a frequency of 100 Hz)

Compositions	Dopants (0.5 at%)	Dielectric constant	Dissipation factor
3/52/48	Undoped	1508	0.0157
	Gd_2O_3	1430	0.0261
	Nb_2O_5	1590	0.0179
4/48/52	Undoped	960	0.0114
	Gd_2O_3	1005	0.0310
	Nb_2O_5	1190	0.0258
5/54/46	Undoped	2032	0.0194
	Gd_2O_3	2125	0.0233
	Nb_2O_5	2206	0.0201

4.4.2 Piezoelectric properties

The piezoelectric constants (d_{33}) of the poled samples, which were measured with a Piezo d-meter (Berlincourt model CADT), were listed in Table 4.5. The piezoelectric constant had the same tendency with the dielectric constant data. The dielectric constant (K) and piezoelectric constant (d_{33}) are plotted as functions of compositions and dopants in PLZT ceramics as shown in Fig.4.16.

Table 4.5 Piezoelectric constant (d_{33}) of the PLZT samples

Compositions	Dopants (0.5 at%)	Piezoelectric constant (d_{33}, pC/N)
3/52/48	Undoped	270
	Gd_2O_3	300
	Nb_2O_5	335
4/48/52	Undoped	200
	Gd_2O_3	205
	Nb_2O_5	225
5/54/46	Undoped	392
	Gd_2O_3	416
	Nb_2O_5	422

From the results obtained, it was found that the dielectric constant (K) and piezoelectric constant (d_{33}) were related to each other. As illustrated in Fig.4.16, high dielectric constant samples were also found to have large piezoelectric constant. The maximum dielectric and piezoelectric constants were found in Nb_2O_5 doped PLZT 5/54/46 ceramic. They were 2206 and 422 pC/N, respectively.

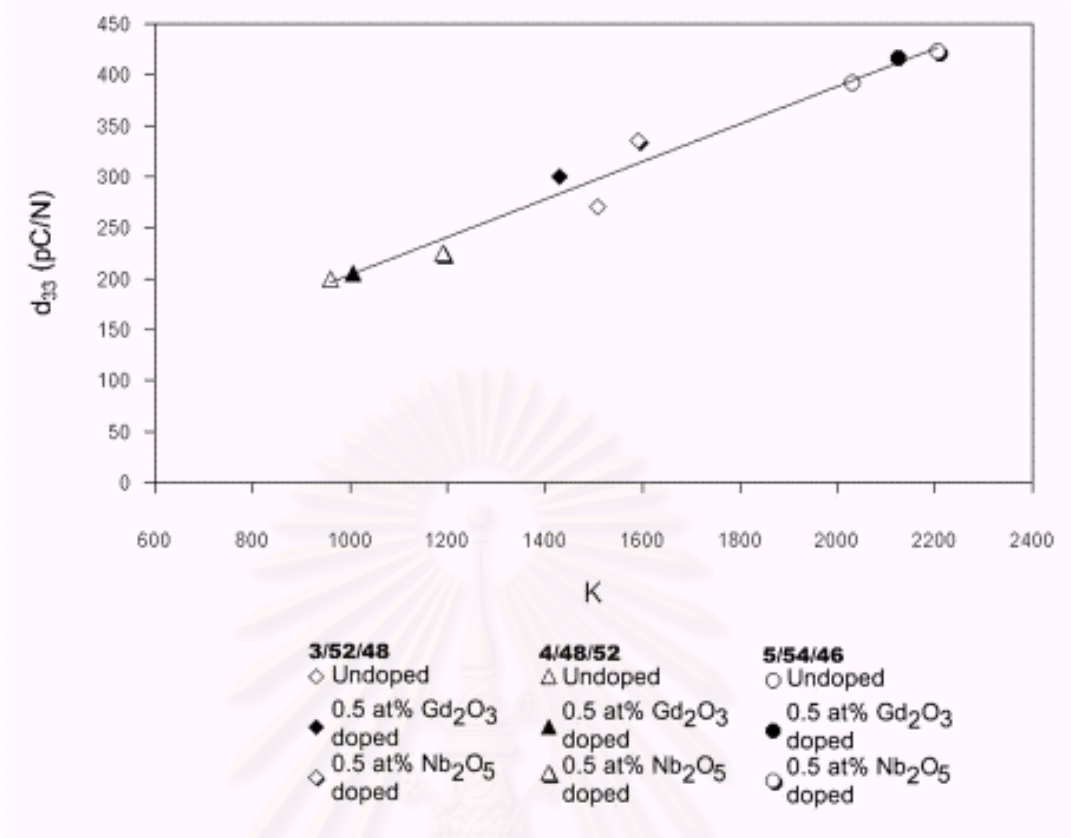

Fig.4.16 The relation between dielectric constant (K) and piezoelectric constant (d_{33}) of poled PLZT samples

In this study, Nb_2O_5 was considered as a B-site donor which replaced Zr^{4+} or Ti^{4+} ions. This type of doping was a soft doping which softened the properties of PLZT materials. It increased the dielectric constant while the coercive field was reduced. Gd_2O_3 was considered as a B-site accepter which was a hard doping. This type of doping inhibited the domain motion, it followed with the increase in coercive field. Therefore, under the same poling conditions, PLZT doped with Nb_2O_5 which had the lower coercive field exhibited better properties than PLZT doped with Gd_2O_3.

4.5 Photovoltage and Photocurrent Measurement

The plot between the applied voltage and the measured current was used to calculate generated photocurrent and photovoltage of the sample specimens. The photovoltage (E_{ph}) was determined from the intercept of the horizontal applied voltage axis while the photocurrent (I_{ph}) was determined from the intercept of the vertical measured current axis. Photoconductance (G_{ph}) of the sample was calculated using the relation

$$E_{ph} = \frac{I_{ph}}{G_{ph}} \qquad (4.1)$$

Photovoltaic properties of all the samples are listed in Table 4.6.

Table 4.6 Photocurrent and photovoltage of PLZT samples
(Light intensity 2.1 mW/cm^2)

Compositions	Dopants (0.5 at%)	I_{ph} (nA/cm)	E_{ph} (V/cm)	G_{ph} (10^{-12} A/V)
3/52/48	Undoped	0.55	303.37	1.81
	Gd_2O_3	0.51	313.21	1.63
	Nb_2O_5	0.41	424.44	0.97
4/48/52	Undoped	1.15	306.06	3.76
	Gd_2O_3	0.57	324.69	1.76
	Nb_2O_5	0.71	454.69	1.56
5/54/46	Undoped	0.23	373.64	0.62
	Gd_2O_3	0.18	452.90	0.40
	Nb_2O_5	0.19	512.32	0.37

The above data show that dopants have no positive effect on photocurrent. This can be seen from the decreasing in photocurrent of doped PLZT samples in all compositions. However, PLZT 4/48/52 provided the maximum photocurrent while the minimum was presented in PLZT 5/54/46. This finding agreed with the previous study by Poosanaas P. and Uchino K [Poosanaas P. and Uchino K. (1999)][1].

Unlike the photocurrent, dopants showed a significant effect on the photovoltage of PLZT ceramics. It was found that Nb_2O_3 enhanced photovoltage of PLZT ceramics more than Gd_2O_3.

Composition of PLZT was also found to play an important role on the photovoltage of PLZT. PLZT 5/54/46 was found to provide the lowest photocurrent but the highest photovoltage. The results of this study supported the previous study [Poosanaas P. and Uchino K. (1999)][1]. However, PLZT 3/52/48, which was reported in many previous studies to have a good photostrictive property, did not exhibit either high photocurrent or photovoltage as shown in Fig.4.17.

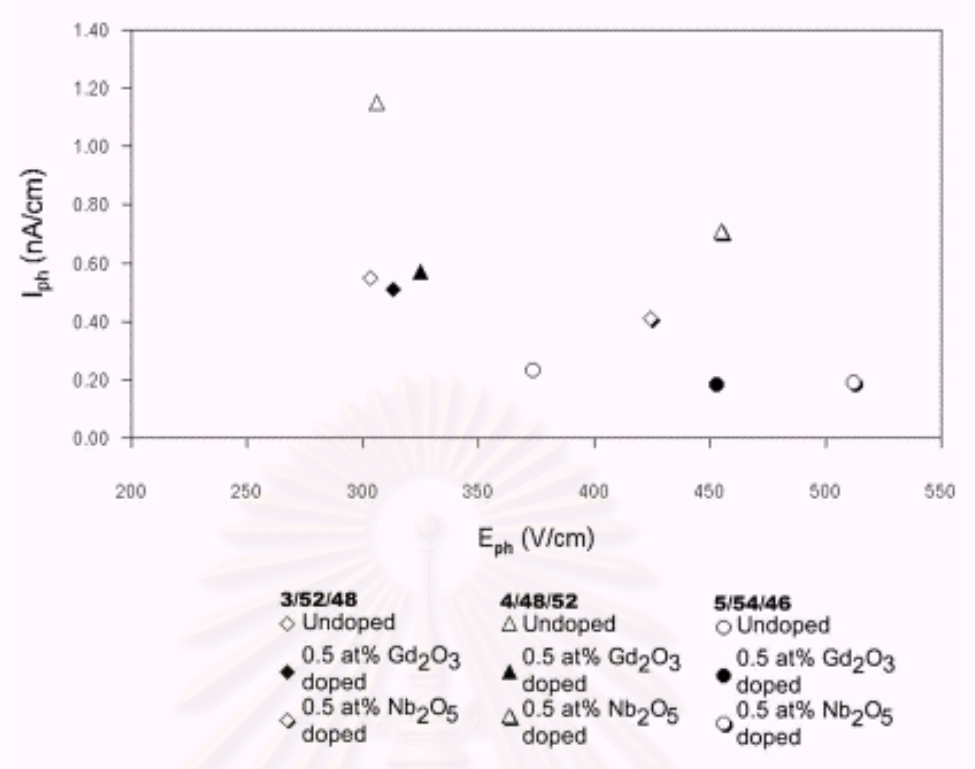

Fig.4.17 I_{ph} as a function of E_{ph} of PLZT samples

As illustrated in Fig.4.17, it is not necessary that high photocurrent sample will give high photovoltage. This can be implied that composition and dopants were the main factors that controlled these properties.

Photoconductance of PLZT samples showed the same trend as photocurrent. This is because the generated current was strongly affected by material conductivity (on the other hand, resistivity). To illustrate the relation between photoconductance and photocurrent (equation 4.1), these two values are plotted and shown in Fig.4.18.

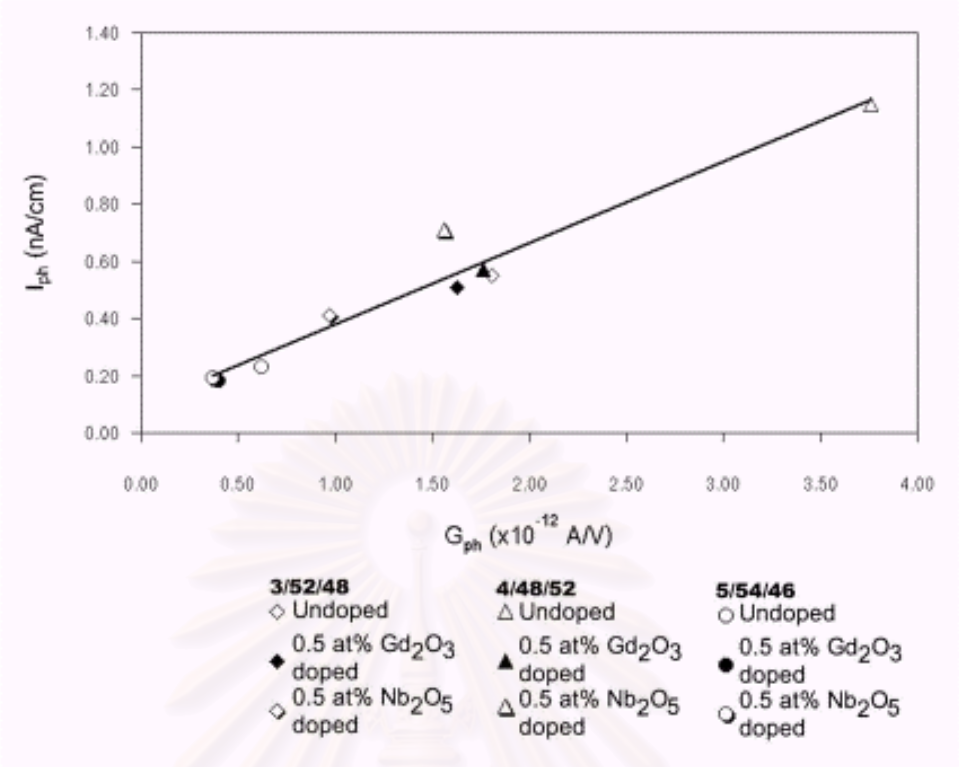

Fig.4.18 I_{ph} as a function of G_{ph} of PLZT samples

Photovoltage and photoconductance were also related through equation 4.1. Photovoltage was inversely proportional to photoconductance as shown in Fig.4.19 where photovoltage is plotted as a function of photoconductance.

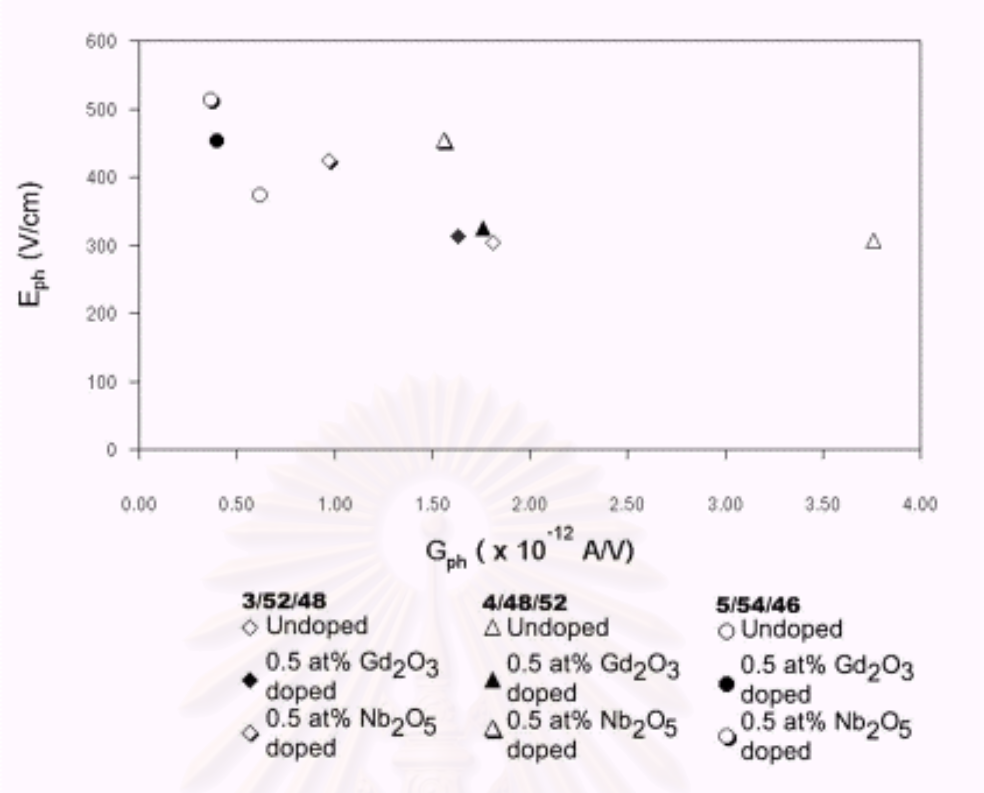

Fig.4.19 E_{ph} as a function of G_{ph} of PLZT samples

Considering tetragonality of PLZT samples listed in Table 4.1, it was shown that photocurrent and tetragonality increased in the same direction as shown in Fig 4.20. This figure shows that the data are obviously divided into three groups. The composition with high tetragonality provided high photocurrent. This can be concluded that tetragonality of PLZT ceramics had some effect on photocurrent.

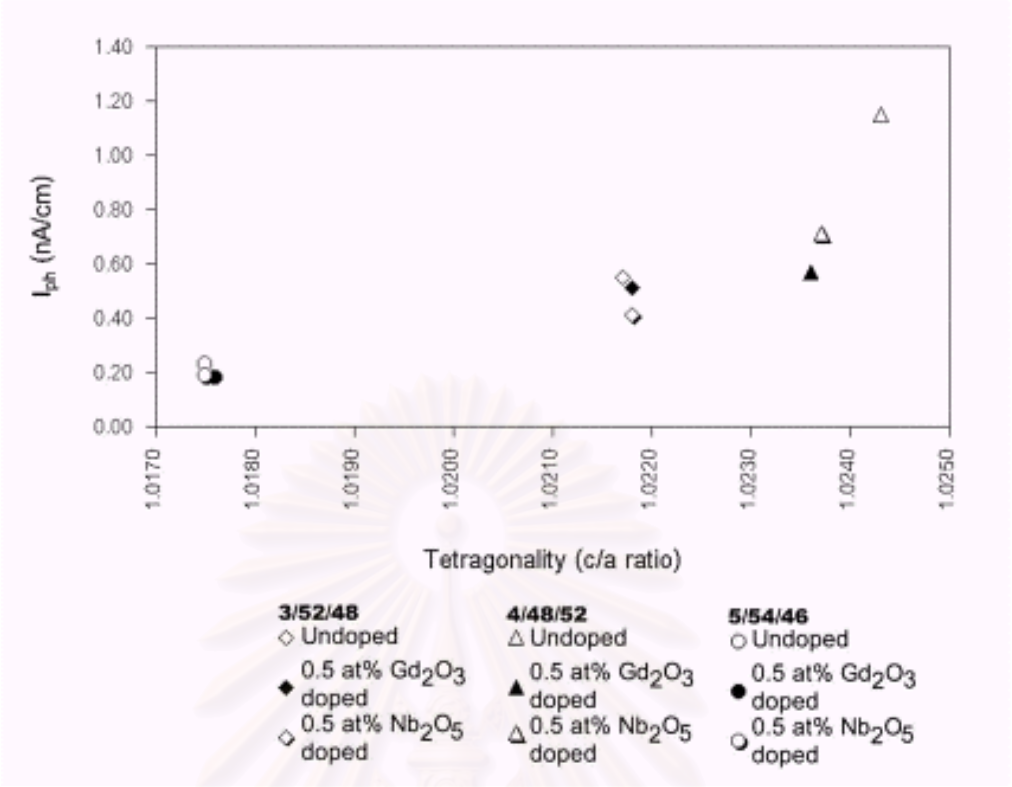

Fig.4.20 I_{ph} as a function of Tetragonality

In addition, figure of merit for response speed ($d_{33}I_{ph}/C$) and magnitude of strain (d_{33} x E_{ph} or X_{ph}) were calculated and displayed in Table 4.7.

Table 4.7 the merit of response speed and magnitude of strain

Compositions	Dopants (0.5 at%)	X_{ph} (%)	$d_{33}xI_{ph}/C$ (t^{-1})
3/52/48	Undoped	0.8191	$4.68x10^{-07}$
	Gd_2O_3	0.9396	$5.45x10^{-07}$
	Nb_2O_5	1.4219	$4.10x10^{-07}$
4/48/52	Undoped	0.6121	$13.18x10^{-07}$
	Gd_2O_3	0.6656	$6.14x10^{-07}$
	Nb_2O_5	1.0231	$6.16x10^{-07}$
5/54/46	Undoped	1.4647	$2.19x10^{-07}$
	Gd_2O_3	1.8841	$1.92x10^{-07}$
	Nb_2O_5	2.1620	$1.80x10^{-07}$

The merit of response speed was obtained for PLZT 4/48/52 ceramic due to its high photocurrent, low capacitance and high c/a ratio. The merit of photo-induced strain was found in PLZT 5/54/46 doped with Nb_2O_5, which displayed high values of dielectric constant and photovoltage. This meant that PLZT 4/48/52 is suitable for high responsed speed applications, such as vibrators or photophone, while Nb_2O_5 doped PLZT 5/54/46 ceramics should be selected for high photo-induced strain applications. Because of these two merits were presented in different composition, it is interesting to develop materials which has optimum properties, fast response and high strain.

4.6 Fabrication of photostrictive devices

Sintered samples were cut into 3 mm x 6 mm x 1 mm, the same dimensions as for photovoltage and photocurrent measurements. The samples were electroded and poled in silicone oil at 120^{o}C under 2 kV/mm electric field for 15 min.

The poled samples were connected together to fabricate the devices, power supply and micro-walker. Photovoltage and photocurrent of these devices were measured by applying voltage between –100 and +100 V and detecting the current (electrometer Keithley 617) during illuminating the devices.

4.6.1 Photocurrent power supply

Undoped PLZT 4/48/52, which displayed the highest photocurrent, was selected to fabricate the photocurrent power supply.

The poled, rectangular shape samples (3 x 6 x 1 mm.) were connected together using parallel circuit to increase the generated current. The design of photocurrent power supply is illustrated in Fig.4.21.

The circuit consists of six pieces of rectangular shape samples were stuck with three thin copper plates by conductive silver glue. These six pieces of samples were divided into 2 parts, the upper and lower part. Each part consisted of three samples. The negative poles of the samples attached with the copper plate number 3 while the positive poles connected with the copper plates number 1 and 2. The equivalent electric circuit of this device is also displayed in Fig.4.21.

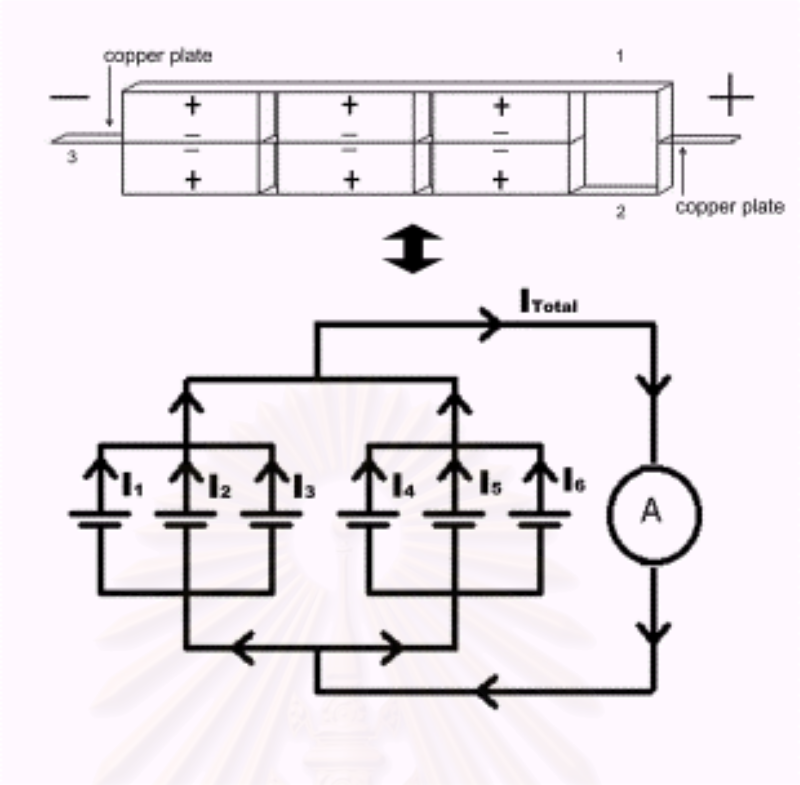

Fig.4.21 The design of photocurrent power supply and its equivalent circuit

By using the parallel circuit, the photocurrent, which generated in each sample when illuminated, will be combined together. This combination can be summarized as follow:

$$I_{Total} = I_1+I_2+I_3+I_4+I_5+I_6$$

This assumption was proved by directly measured the current generated from the device. The photocurrent of each PLZT 4/48/52 sample is 1.05, 1.13, 1.04, 1.15, 0.98 and 1.01 nA/cm and the photocurrent of the device is 6.16 nA/cm. This result agreed with the above equation.

This design can be expanded to generate more photocurrent by increasing the size and the number of PLZT samples. However, photocurrent

supplied by this device showed some electrical lost which may be caused by the contact between the samples and the copper plates.

4.6.2 Micro-walker device

Due to its high piezoelectric constant (d_{33}) and photovoltage (E_{ph}), PLZT 5/54/46 doped with Nb_2O_5 was selected for a micro-walker device which was designed into a simple shape using the poled rectangular-shape samples. Samples with similar dimension to 4.6.1 were stucked together into a row as a micro-walker's body using the conductive silver glue. These connected samples were equivalent to a series circuit of which the voltage was combined along the electric lead wires as shown in Fig.4.22.

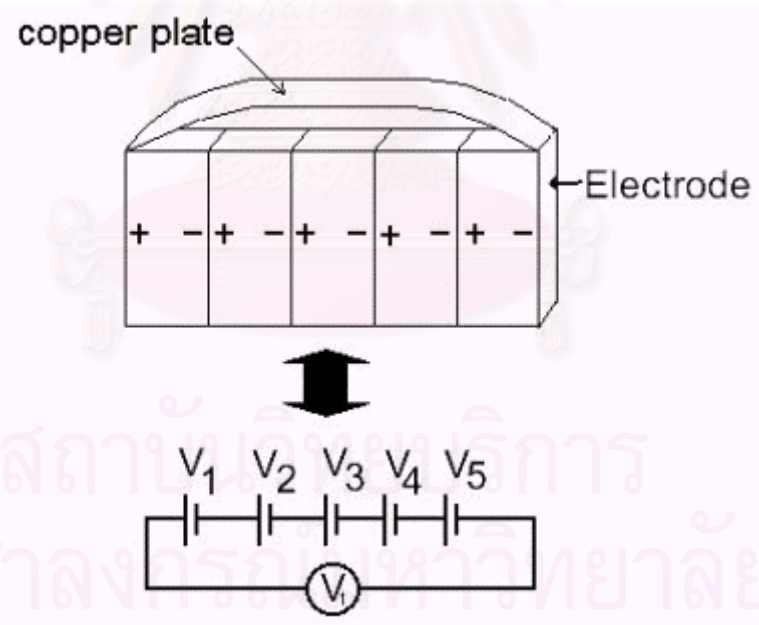

Fig.4.22 The design of micro-walker's body

Both ends of the body were joined with two legs and the thin copper plate as shown in Fig.4.23. A thin plastic plate was cut into two small pieces (5 x 23 x 2 mm.) for its legs. The two small glass plates were attached at both ends of the legs to act as the nails. These inclined nails were used to control the movement direction of the device to be forwarded.

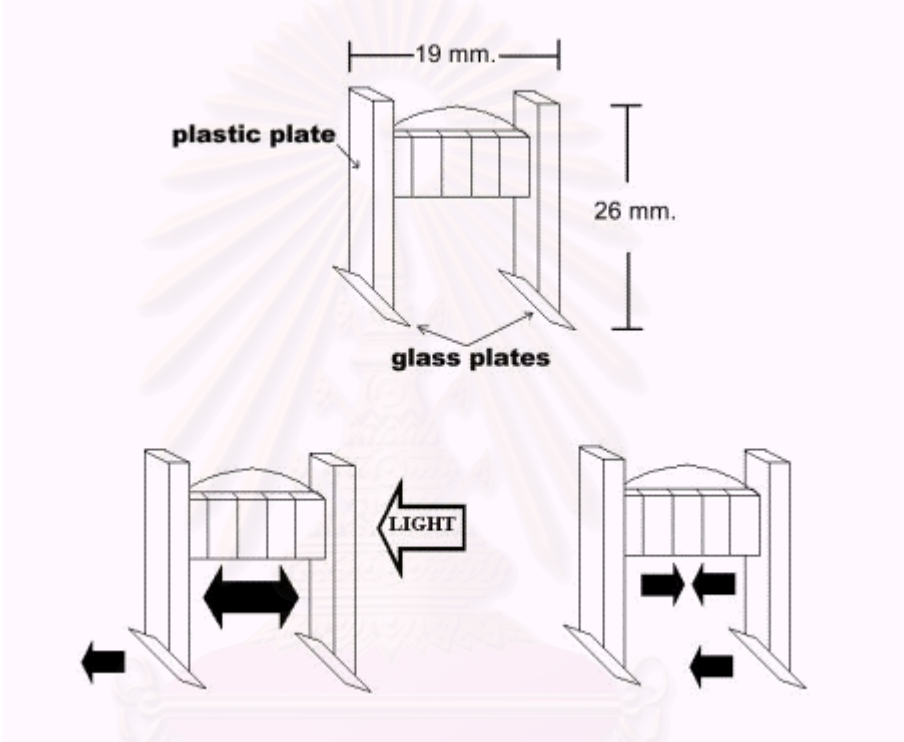

Fig.4.23 The design of micro-walker device

By using the series circuit, the generated photovoltage in each sample was supposed to be combined together and displayed into the total photovoltage. The generated photovoltage in each sample was 510.25, 498.50, 502.36, 495.35 and 512.20 V/cm. However, the total photovoltage directly detected from the stack of samples was 1956.35 V/cm. This result showed high electrical lost due to the contact between each sample.

A chopper of light illumination was used to control the movement of this device. While the body of micro-walker was illuminated on, it was expanded via the photostrictive mechanism and the front leg was pushed forward. When the incident light was cut off, the body was contracted and the back leg start to move. Due to the small photo-induced strain (in the range of micron), it was impossible to observe the movement of the device. However, this micro-walker was lie the basic idea on photostrictive mechanism which is small in size and weight (1.35 g) and the ability to sense and get actuated itself.

CHAPTER 5
CONCLUSIONS

The goal of this research is to study high induced strain and fast response speed PLZT ceramics via composition and dopant type as well as fabricate the photostrictive devices from the suitable PLZT ceramics.

The properties of photostrictive PLZT ceramics were investigated through the doping effect of Nb_2O_5 and Gd_2O_3 on PLZT (3/52/48), (4/48/52) and (5/54/46) compositions. The results can be summarized as follows:

1. The dielectric constant and piezoelectric constant were related to each other. High dielectric constant PLZT ceramic was found to have large piezoelectric constant.

2. Nb_2O_5 dopant at 0.5 at % concentration showed the positive effects on the properties of PLZT ceramics. It increased the dielectric constant, piezoelectric constant and enhanced photovoltage 10-40% as compared to undoped PLZT ceramics.

3. Undoped PLZT (4/48/52) ceramics providing high photocurrent with low dielectric constant made it suitable for high response speed applications, such as vibrators or photo-acoustic devices. Due to this reason, it was selected to be fabricated into a photocurrent power supply device. This device was designed into a parallel circuit to enhance the generated photocurrent. The generated photocurrent increased with the number of PLZT samples connected in the parallel.

4. Nb_2O_5 doped PLZT (5/54/46) ceramic displayed high dielectric constant, piezoelectric constant, and photovoltage which made it suitable for high displacement applications, such as photo-driven robot. Due to its high induced-strain, it was selected to fabricate as a micro-walker. PLZT samples were connected together in a series circuit to make them as a micro-walker's body. The generated photovoltage increased with the number of PLZT samples connected in the series.

CHAPTER 6
SUGGESTIONS FOR FUTURE WORKS

The photostrictive device will be a prototype for a micro devices which is small in size, inexpensive and have the ability to sense and get actuated itself. This research is the result of the coupling of electrical, optical and mechanical fields and serves as a useful guideline for new materials, i.e. sensors and actuators.

Suggestions for future research are listed as follows:

1. PLZT photostrictive ceramics have the ability to transduce Ultraviolet light into the electric current. Therefore, it is promising to develop this material as a UV sensor which can sense and detect the intensity of UV light.
2. Micro-walker driven by the irradiation of light has drawn a considerable attention. However, the limitation of this device is the movement in micron range. It would be worthwhile to enhance the magnitude of strain by designing this PLZT ceramics into a unimorp or bimorph shape.
3. Since the maximum photocurrent and photovoltage were obtained at different compositions of PLZT ceramics, the further investigation through the compositions and dopants for the optimum high response speed and induced strain will be necessary.
4. The resonance frequency of PLZT (5/54/46) doped with Nb_2O_5 should be examined in order to maximize the displacement

REFERENCES

1) Poosanaas P. and Uchino K., Photostrictive Effect in Lanthanum-Modified Lead Zirconate Titanate Ceramics near the Morphotropic Phase Boundary, Materials chemistry and Physics 61 (1999): 36-41.

2) Haertling G.H. and Land C.E., Hot-Pressed (Pb,La)-(Zr,Ti)O3 ferroelectric Ceramics for Applications, J. Am. Ceram. Soc. 54 (1971): 1-11.

3) Haerthling G.H. and Land C.E., Recent Improvements in the Optical and Electrooptic Properties of PLZT ceramics, Ferroelectrics 3 (1972): 269-280.

4) Buchanan R.C., Ceramic Materials for Electronics, 2nd ed. Mareel Dekker, IN(1991): 144-146.

5) Duram P. and Moure C., High Density PLZT Ceramics Prepared Chemically from Different Raw Materials, Am. Ceram. Soc. Bull. 64 (1985): 575-79.

6) Hardtl K.H. and Hennings D., Distribution of A-site and B-site Vacancies in (Pb,La)-(Ti,Zr)O3 Ceramics, J. Am. Ceram. Soc. 55 (1972): 230-231.

7) Henning D. and Hardtl K.H., Distribution of Vacancies of Lanthan-Doped Lead Titanate, Phys.Status Solid A 3(1970): 465-74.

8) Meitzler A.H. and O' Bryan H.M., Jr., Polymorplism and Penferroelectricity in PLZT Ceramics, Proeeding of the IEEE 61 (1973): 1-3.

9) Tjhen W., Tamagawa T., Ye C.P., Hsuch C.C., Schiller P., and Polla D.L., Properties of Piezoeletric Thin Films For Micromechanical Devices and Systems, Proeeding of the IEEE, CH2957-9 (1991).

10) Nonaka K., Akiyama M.,Hagio T. and Takase A., Bulk photovoltaic Effect in Reduced/Oxidized Lead Lanthanum Titanate Zirconate Ceramics, Jpn. J. Appl. Phys. 34 (1995).

11) Uchino K., New applications of Photostrictive ferroics, Mat Res Innovat, 1 (1997): 163-168.

12. Tanimura M. and Uchino K. Effect of Impurity Doping on Photostriction in Ferroelectric Ceramics, Sensors and Materials ,1 (1988): 47-56.

13. Atkin R.B. and M.F.Richard,Point Defects and Sintering of Lead Zirconate-Titanate, J. Am. Ceram. Soc, 54 (1971): 265-270.

14) Yuhuan Xu, Cheng C.H. and Mackenzie J.D.,Electrical Characterizations of Polycrystalline and Amorphous Thin Films of $Pb(Zr_xTi_{1-y})O_3$ and $BaTiO_3$ Prepared by Sol-Gel Technique, Journal of Non- crystalline solids, 176(1994): 1-17.

15) Tani T., Asai M., Takatori K. and Kamiya N., Evaluation of Dielectric Strength and Breakdown Behavior for Sr-Nb- Doped PZT Ceramics with Various Shapes of Electrodes, Journal of the ceramic Society of Japan 105 (1997): 308-311.

16) Neurgaonkar, Ratnakar R.,Oliver, John R.,Nelson and Jeffry G., Nb-Doped PLZT Piezoelectric Ceramics, United States Patent :5,595,677, (1997): 1-7.

17) Poosanaas P. Photovoltaic and Photostrictive Effects in Lanthanum-Modified Lead Zirconate Titanate Ceramics, A thesis in Materials.,The Pennsylvania State University, (1999): 31-32.

18) Yuhuan Xu, Ferroelectric Materials and Their Applications, 1st ed., Elsevier, Amsterdam (1991).

19) Uchino K., New applications of photostrictive ferroics, Mat Res Innovat, 1 (1997): 163-168.

20) Uchino K.,Feroelectric Devices, Marcel Dekker, (2000): 170.

21) Randall, C. A.; Kim, N.; Kucera, J. P.; Cao, W.; and Shrout, T. R. Intrinsic and Extrinsic Size Effects in Fine-Grained Morphotropic-Phase-Boundary Lead Zirconate Titanate Ceramics. J. Am. Ceram. Soc. 81 (1998): 677-688.

22) Sakai T. and Kawamoto H. Relationship between Electrical Properties and Dynamic Displacement of Piezoelectric Pellets. J. Ceram. Soc. Jpn. 105 (1997): 1210-1215.

23) Uchino K. and Poosanaas P., Photostriction in PLZT and its Applications. CIMTEC' 98 Invited Paper (1998): 1-12.

24) Park, H. B., Park, C. Y., Hong, Y. S., Kim, K. and Kim, S. J., Structural and Dielectric Properties of PLZT Ceramics Modified with Lanthanide Ions, J. Am. Ceram. Soc., 82 (1999): 94-102.

APPENDICES

APPENDIX A

JCPDS CARD FOR X-RAY DIFFRACTION DATA

05-0570 Wavelength= 1.5405 *

PbO

Lead Oxide

Massicot, syn

Rad.: CuKa1 λ: 1.5405 Filter: Ni Beta□M d-sp:

Cut off: Int.: Diffract. I/Icor.: 6.60

Ref: Swanson, Fuyat, Natl. Bur. Stand. (U.S.), Circ. 539, 2, 32 (1953)

Sys.: Orthorhombic S.G.: Pbma (57)

a: 5.489 b: 4.755 c: 5.891 A: 1.1544 C: 1.2389

α: β: γ: Z: 4 mp:

Ref: Kay, Acta Crystallogr., 14, 80 (1961)

Dx: 9.642 Dm: 9.642 SS/FOM$_{38}$=29(.0157, 66)

Color: Yellow
X-ray pattern at 27 C. Sample from National Lead Company. CAS #: 1317-36-8. Spectroscopic analysis: <0.01% Bi, Fe; <0.001% Al, Ag, Cu, Mg, Si, Ca. Other form, litharge. O Pb type. C.D. Cell: a=5.489, b=5.891, c=4.755, a/b=0.9318, c/b=0.8072, S.G.=Pcam(57). PSC: oP8. Deleted by 38-1477. Mwt: 223.20. Volume[CD]: 153.76.

2θ	Int	h	k	l	2θ	Int	h	k	l
15.021*	6	0	0	1	80.836*	3	4	2	0
29.090*	100	1	1	1	82.005*	4	3	3	1
30.313*	31	0	0	2	85.103*	2	2	2	4
32.604*	28	2	0	0	86.900*	2	1	1	5
35.994*	<1	2	0	1	88.687*	4	4	2	2
37.815*	20	2	1	0	89.821*	2	2	4	0
39.525*	<1	1	1	2					
40.930*	<1	2	1	1					
45.113*	12	2	0	2					
46.206*	2	0	0	3					
49.209*	14	0	2	2					
50.761*	14	2	2	0					
53.075*	15	1	1	3					
56.025*	13	3	1	1					
57.712*	<1	2	0	3					
60.281*	9	2	2	2					
61.161*	2	0	2	3					
63.008*	11	1	3	1					
66.330*	<1	3	2	1					
68.306*	1	4	0	0					
68.820*	<1	1	1	4					
71.087*	1	2	2	3					
72.864*	2	2	0	4					
73.390*	3	3	1	3					
75.935*	2	0	2	4					
76.511*	2	2	3	2					
79.625*	4	1	3	3					

05-0602 Wavelength= 1.5405 *

La2O3

Lanthanum Oxide

Rad.: CuKa1 λ: 1.5405 Filter: Ni Beta M d-sp:

Cut off: Int.: Diffract. I/Icor.:

Ref: Swanson, Fuyat, Natl. Bur. Stand. (U.S.), Circ. 539, III, 33 (1954)

Sys.: Hexagonal S.G.: P$\bar{3}$m1 (164)

a: 3.9373 b: c: 6.1299 A: C: 1.5569

α: β: γ: Z: 1 mp:

Ref: Ibid.

Dx: 6.574 Dm: SS/FOM: F$_{30}$=47(.0160, 40)

Color: Colorless
Pattern taken at 26 C. Sample from Fairmount Chemical Company. Sample was annealed at 1200 C for one hour and mounted in petrolatum to prevent reabsorption of C O2 + H2 O. Spectroscopic analysis: <0.01% Ca, Mg, Si: <0.001% Al, Cu, Fe, Pb. Merck Index, 8th Ed., p. 608. Opaque mineral optical data on specimen from Nanseke, Uganda: R3R%=14.2, Disp.=Std., VHN100=782-813. Ref.: IMA Commission on Ore Microscopy QDF. Pattern reviewed by Holzer, J., McCarthy, G., North Dakota State Univ., Fargo, ND, USA. ICDD Grant-in-Aid (1990. Validated by calculated pattern except for the following: 2.278 23 102; 1.968 28 110; 1.753 23 103. Calculated pattern indicates that the following reflections might be observable: 6.130 <1 001; 2.043 <1 003; 1.8744 <1 111; 1.4177 <1 113; 1.2260 <1 005. La2 O3 type. PSC: hP5. Mwt: 325.81. Volume[CD]: 82.30.

2θ	Int	h	k	l	2θ	Int	h	k	l
26.109°	34	1	0	0	130.547	2	1	0	7
29.129°	31	0	0	2	131.649	1	4	0	1
29.959°	100	1	0	1	136.844	2	2	2	4
39.525°	58	1	0	2	146.207	1	3	1	4
46.082°	63	1	1	0	148.296	2	2	1	6
52.130°	52	1	0	3					
53.713°	4	2	0	0					
55.437°	24	1	1	2					
55.951°	17	2	0	1					
60.367°	3	0	0	4					
62.255°	5	2	0	2					
66.867°	2	1	0	4					
72.091°	7	2	0	3					
73.390°	2	2	1	0					
75.298°	12	2	1	1					
79.151°	6	1	1	4					
80.844°	4	2	1	2					
83.761°	4	1	0	5					
85.047°	2	2	0	4					
85.316°	4	3	0	0					
89.916°	7	2	1	3					
92.555°	4	3	0	2					
97.818°	<1	0	0	6					
101.423	3	2	0	5					
103.031	3	2	2	0					
103.815	1	1	0	6					
109.037	<1	3	1	0					
110.543	3	2	2	2					
111.023	5	3	1	1					
115.035	2	3	0	4					
116.256	2	1	1	6					
120.248	5	2	1	5					
122.967	1	2	0	6					
127.640	4	3	1	3					

37-1484 Wavelength= 1.5405981 *

ZrO2

Zirconium Oxide

Baddeleyite, syn

Rad.: CuKa1 λ: 1.5405 Filter: Graph Mono Sp: Diffractometer

Cut off: 17.7 Int.: Diffract. I/Icor.: 2.6

Ref: McMurdie, H et al., Powder Diffraction, 1, 275 (1986)

Sys.: Monoclinic S.G.: $P2_1/a$ (14)

a: 5.3129(4) b: 5.2125(4) c: 5.1471(5) A: 1.0193 C: 0.9875

α: β: 99.218(8) γ: Z: 4 mp:

Ref: Ibid.

Dx: 5.817 Dm: SS/FOM$_{30}$=111(.0073, 37)

Color: Colorless
Peak height intensity. The mean temperature of the data collection was 25.5°. Sample was obtained from Titanium Alloy Manufacturing Co. (1990) and was heated to 1300° for 48 hours. CAS #: 1314-23-4. Spectrographic analysis showed that this sample contained less than 0.01% each of Al, Hf and Mg and between 0.1 and 0.01% each of Fe, Si and Ti. Pattern reviewed by Holzer, J., McCarthy, G., North Dakota State Univ., Fargo, ND, USA, ICDD Grant-in-Aid (1990). Agrees well with experimental and calculated patterns. Additional weak reflections [indicated by brackets] were observed. $\sigma(I_{obs})$= ±1. There are a number of polymorphic forms of Zr O2 stable at different temperatures and pressures. The structure of Zr O2 (baddeleyite) was determined by McCullough and Trueblood (1) and confirmed by Smith and Newkirk (2). O2 Zr type. Also called: zirconium dioxide.Also called: zirkite.Silver, fluorophlogopite used as an internal stands. PSC: mP12. To replace 13-307 and 36-420 and validated by calculated pattern 24-1165. Mwt: 123.22. Volume[CD]: 140.70.

2θ	Int	h	k	l
17.419*	3	0	0	1
24.048*	14	1	1	0
24.441*	10	0	1	1
28.175*	100	$\bar{1}$	1	1
31.468*	68	1	1	1
34.160*	21	2	0	0
34.382*	11	0	2	0
35.309*	13	0	0	2
35.900*	2	$\bar{2}$	0	1
38.396	1	[$\bar{2}$	1	0]
38.541*	4	1	2	0
39.411*	<1	0	1	2
39.990*	<1	$\bar{2}$	1	1
40.725*	12	$\bar{1}$	1	2
41.150*	5	2	0	1
41.374*	5	$\bar{1}$	2	1
44.826*	7	2	1	1
45.522*	6	$\bar{2}$	0	2
48.949*	2	$\bar{2}$	1	2
49.266*	18	2	2	0
50.116*	22	0	2	2
50.559*	13	$\bar{2}$	2	1
51.193*	5	$\bar{1}$	2	2
54.104*	11	0	0	3
54.680*	<1	2	2	1
55.270	11	[1	2	2]
55.400*	11	3	1	0
55.570*	9	$\bar{3}$	1	1
55.883*	6	0	3	1
57.168*	7	$\bar{1}$	1	3
57.861*	4	$\bar{1}$	3	1
58.268*	3	$\bar{2}$	2	2
59.775*	8	1	3	1
60.055*	7	$\bar{2}$	0	3
61.367*	5	3	1	1
61.984*	5	$\bar{3}$	1	2
62.838*	8	1	1	3
64.079*	1	3	2	0
64.250*	2	2	3	0
64.966*	<1	0	3	2
65.384*	2	$\bar{2}$	3	1
65.700*	6	0	2	3
65.884*	4	$\bar{1}$	3	2
68.912*	1	2	3	1
69.620*	<1	3	2	1
70.190*	<1	$\bar{3}$	2	2
71.071*	2	$\bar{2}$	2	3
71.300*	4	$\bar{4}$	0	1
71.950*	1	4	0	0
72.104*	1	$\bar{2}$	3	2
72.450*	<1	0	4	0
72.642*	<1	3	1	2
73.580*	<1	$\bar{3}$	1	3
74.682*	2	0	0	4
75.046*	4	1	4	0
76.410*	1	$\bar{1}$	1	4
77.392*	<1	3	3	0
78.079*	<1	4	0	1
78.866*	1	0	3	3

04-0477 Wavelength= 1.54056 i

TiO2

Titanium Oxide

Anatase, syn

Rad.: CuKa1 λ: 1.5405 Filter: Ni Beta M d-sp: Diffractometer

Cut off: Int.: Diffract. I/Icor.:

Ref: Swanson, Tatge, Private Communication, (1950)

Sys.: Tetragonal S.G.: $I4_1/amd$ (141)

a: 3.783 b: c: 9.51 A: C: 2.5139

α: β: γ: Z: 4 mp:

Ref: Ibid.

Dx: 3.899 Dm: SS/FOM$_{25}$=8(.062, 48)

PSC: tI12. Mwt: 79.90. Volume[CD]: 136.10.

2θ	Int	h	k	l
25.354*	100	1	0	1
36.883*	9	1	0	3
37.784*	22	0	0	4
38.506*	9	1	1	2
48.076*	33	2	0	0
53.921*	21	1	0	5
55.114*	19	2	1	1
62.073*	4	2	1	3
62.726*	13	2	0	4
68.594*	5	1	1	6
70.357*	5	2	2	0
75.092*	10	2	1	5
76.082*	3	3	0	1
82.264*	2	3	0	3
83.138*	3	3	1	2
90.258*	3			
95.176*	3	3	2	1
98.433*	2	1	0	9
107.525	4	3	1	6
109.009	3	4	0	0
113.914	2	3	2	5
118.563	3	1	1	10
120.391	2	2	2	8
135.889	<1	3	2	7
137.384	3	4	1	5
143.965	1	3	0	9
149.183	3			

33-0784 Wavelength= 1.5418

Pb(Zr0.52Ti0.48)O3

Lead Zirconium Titanium Oxide

Rad.: CuKa λ: 1.5418 Filter: Ni Beta□M d-sp: Diffractometer

Cut off: Int.: Diffract. I/Icor.:

Ref: Kakegawa, K. et al., Solid State Commun., 24, 769 (1977)

Sys.: Tetragonal S.G.:

a: 4.036 b: c: 4.146 A: C: 1.0273

α: β: γ: Z: 1 mp:

Ref: Ibid.

Dx: 8.006 Dm: SS/FOM$_{30}$=15(.060, 34)

Color: Light yellow
No composition fluctuation. Silicon used as an internal stand. Mwt: 325.62. Volume[CD]: 67.54.

2θ	Int	h	k	l	2θ	Int	h	k	l
21.432*	9	0	0	1	78.379*	2	3	1	1
22.023*	12	1	0	0	85.099*	4	2	0	3
30.942*	100	1	0	1	86.034*	4	3	0	2
31.387*	100	1	1	0	86.992*	4	3	2	0
38.283*	15	1	1	1	88.985*	15	1	2	3
43.663*	9	0	0	2	90.023*	15	3	1	2
44.917*	16	2	0	0	91.089*	15	3	2	1
49.424*	5	1	0	2	96.092*	<1	0	0	4
50.417*	6	2	0	1	99.627*	<1	4	0	0
50.417*	6	2	1	0	100.319	<1	1	0	4
53.390*	5				101.881	<1	2	2	3
54.734*	12	1	1	2	102.991	1	3	2	2
55.524*	24	2	1	1	104.602	2	1	1	4
64.434*	9	0	2	2	106.185	2	3	0	3
65.398*	5	2	2	0	107.981	4	4	1	1
67.810*	2	0	0	3	108.313	4	3	3	0
69.002*	6	2	1	2	110.595	1	1	3	3
69.645*	6	2	2	1	112.473	<1	3	3	1
69.645*	6	3	0	0	113.446	2	2	0	4
72.225*	6	1	0	3	116.411	6	4	0	2
74.065*	9	3	0	1	117.235	6	4	2	0
74.065*	9	3	1	0	118.076	6	1	2	4
76.588*	2	1	1	3	121.167	1	4	1	2

2θ	Int	h	k	l
121.862	1	4	2	1
124.798	3	2	3	3
126.131	2	3	3	2
133.607	1	2	2	4
136.843	5	0	0	5
137.195	5	4	2	2
139.685	2	3	0	4

42-0004 Wavelength= 1.5418

PbTiO3

Lead Titanium Oxide

Rad.: CuKa λ: 1.5418 Filter: d-sp:

Cut off: Int.: I/Icor.:

Ref: Uedaira, S., EP 186,199, Eur. Pat. Appl., (1986)

Sys.: Tetragonal S.G.: 1

a: 12.3574(13)* c: 14.534(5) A: C: 1.1761

α: β: γ: Z: mp:

Ref: Ibid.

Dx: Dm: SS/FOM$_{26}$=12(.0197,107)

Cell parameters generated by least squares refinement. Application number: 85116573.8. Reference reports: a=12.34, c=14.5. PSC: tP2. Mwt: 303.10. Volume[CD]: 2219.42.

2θ	Int	h	k	l	2θ	Int	h	k	l
14.330*	22	2	0	0	57.530*	<2	7	2	3
22.760*	55	3	1	0	57.810*	2	5	3	6
24.460*	8	2	1	3	59.620*	2	6	4	4
24.460*	8	0	0	4					
28.910*	22	4	0	0					
30.710*	100	3	3	0					
32.000*	45	3	2	3					
32.400*	12	4	2	0					
35.200*	8	4	1	3					
37.080*	2	5	1	0					
38.200*	6	4	0	4					
41.310*	2	4	4	0					
42.690*	<2	5	3	0					
43.650*	22	5	2	3					
43.950*	16	6	0	0					
46.480*	4	6	2	0					
47.750*	6	4	0	6					
50.150*	<2	4	2	6					
50.150*	<2	0	0	8					
50.930*	6	5	4	3					
52.360*	2	5	5	0					
53.170*	<2	6	2	4					
53.470*	14	6	4	0					
55.400*	20	7	0	3					
56.730*	8	7	3	0					

35-0739 Wavelength= 1.5405981

PbZrO3

Lead Zirconium Oxide

Rad.: CuKa1 λ: 1.5405 Filter: Graph Mono d-sp: Diffractometer

Cut off: 22.1 Int.: Diffract. I/Icor.:

Ref: Natl. Bur. Stand. (U.S.) Monogr. 25, 21, 74 (1984)

Sys.: Orthorhombic S.G.: P2cb (32)

a: 8.2418(1.3) b: 11.7764(13) c: 5.8816(7) A: 0.6990 C: 0.4994

α: β: γ: Z: 8 mp:

Ref: Ibid.

Dx: 8.071 Dm: SS/FOM $_{30}$=44(.0093, 73)

Color: Gray-yellow

Peak height intensity. CAS #: 12060-01-4. The sample was made by heating PbO and Zr O2 together at 900 C overnight. The temperature of data collection was approximately 25.0 C. $d(I_{obs})$= ·1. Above about 150 C Pb Zr O3 is cubic, perovskite type. Earlier this phase was considered tetragonal. Distorted perovskite, Ca O3 Ti type. Silicon used as an internal stand. PSC: oP40. Mwt: 346.42. Volume[CD]: 570.17.

2θ	Int	h	k	l	2θ	Int	h	k	l
16.825*	2	0	1	1	54.016*	30	2	6	1
21.325*	8	0	2	1	54.362*	18	4	0	2
21.559*	5	2	0	0	55.001*	1	4	1	2
27.261*	3	0	3	1	57.026*	2	2	3	3
27.498*	4	2	1	1	57.496*	<1	1	6	1
30.337*	66	0	4	0	59.650*	<1	4	3	2
30.519*	100	2	2	1	61.496*	<1	0	5	3
31.335*	4	0	1	2	63.101*	5	0	8	0
34.059*	<1	0	2	2	63.536*	9	4	4	2
35.041*	<1	2	3	1	65.968*	1	2	5	3
35.751*	<1	1	4	1	66.301*	1	4	1	3
37.523*	14	2	4	0	67.475*	<1	0	6	3
38.201*	2	0	3	2	67.853*	1	4	2	3
38.338*	3	2	1	2	68.084*	2	2	7	2
40.678*	<1	2	2	2	68.348*	2	4	5	2
43.458*	24	0	4	2	68.541*	<1	1	6	3
43.962*	14	4	0	0					
44.298*	2	2	3	2					
46.937*	2	0	1	3					
47.820*	<1	3	4	1					
48.883*	2	0	6	1					
49.005*	2	2	4	2					
49.372*	2	4	2	1					
50.249*	<1	1	2	3					
51.098*	<1	3	3	2					
51.548*	<1	2	6	0					
52.111*	3	0	3	3					
52.224*	4	2	1	3					

APPENDIX B

XRD data of raw oxide mixture of PLZT (3/52/48)

JEOL — Peak search

No.	2-theta	d-value	INT.	I/Io	No.	2-theta	d-value	INT.	I/Io
1	14.960	5.91704	895	28	21	53.120	1.72270	421	13
2	17.560	5.04636	465	14	22	54.640	1.67832	340	11
3	24.000	3.70485	269	8	23	55.960	1.64182	319	10
4	25.240	3.52557	359	11	24	59.720	1.54711	354	11
5	26.440	3.36822	312	10	25	63.080	1.47255	383	12
6	28.160	3.16628	680	21					
7	28.560	3.12284	828	26					
8	29.040	3.07230	1057	33					
9	30.280	2.94925	3213	100					
10	31.360	2.85010	368	11					
11	31.800	2.81166	585	18					
12	32.480	2.75433	324	10					
13	32.560	2.74775	379	12					
14	34.120	2.62560	300	9					
15	35.680	2.51430	812	25					
16	37.840	2.37559	333	10					
17	45.120	2.00777	325	10					
18	46.160	1.96492	349	11					
19	48.520	1.87472	486	15					
20	49.200	1.85039	316	10					

XRD data of PLZT (3/52/48) calcined at different temperatures

Calcined at 850°C for 10 hours

JEOL

No.	2-theta	d-value	INT.	I/Io
1	21.500	4.12966	346	39
2	22.700	3.91399	236	27
3	30.600	2.91913	879	100
4	31.500	2.83775	447	51
5	32.299	2.76935	250	28
6	39.200	2.29625	250	28
7	43.900	2.06069	313	36
8	54.500	1.68230	310	35
9	57.200	1.60914	218	25

Calcined at 950°C for 10 hours

JEOL

No.	2-theta	d-value	INT.	I/Io
1	21.520	4.12587	477	20
2	22.060	4.02608	622	25
3	31.040	2.87875	2443	100
4	31.340	2.85188	1410	58
5	38.360	2.34458	650	27
6	43.800	2.06516	348	14
7	44.900	2.01709	558	23
8	49.740	1.83156	314	13
9	50.540	1.80443	302	12
10	54.960	1.66930	464	19
11	55.500	1.65433	609	25

Sintered at 1250°C for 2 hours

JEOL

No.	2-theta	d-value	INT.	I/Io
1	21.480	4.13346	390	22
2	22.040	4.02969	180	10
3	30.920	2.88965	1791	100
4	31.320	2.85365	555	31
5	38.280	2.34929	501	28
6	43.760	2.06696	363	20
7	44.880	2.01794	345	19
8	49.520	1.83918	282	16
9	50.440	1.80777	189	11
10	54.720	1.67605	353	20
11	55.520	1.65378	482	27

XRD data of PLZT (3/52/48) calcined at 950°C for 10 hours

Undoped

JEOL

No.	2-theta	d-value	INT.	I/Io
1	21.520	4.12587	326	20
2	22.040	4.02969	159	10
3	30.960	2.88601	1624	100
4	31.320	2.85365	529	33
5	38.320	2.34693	448	28
6	43.800	2.06516	360	22
7	44.800	2.02136	329	20
8	49.600	1.83640	270	17
9	50.240	1.81449	179	11
10	54.800	1.67380	390	24
11	55.480	1.65488	497	31
12	64.520	1.44312	264	16

0.5 %at. Gd_2O_3 doped

JEOL

No.	2-theta	d-value	INT.	I/Io
1	21.159	4.19544	375	21
2	21.600	4.11077	235	13
3	30.600	2.91913	1762	100
4	30.920	2.88965	653	37
5	37.960	2.36836	452	26
6	43.480	2.07962	339	19
7	44.480	2.03516	340	19
8	49.280	1.84757	241	14
9	54.560	1.68059	397	23
10	55.160	1.66372	458	26
11	64.240	1.44873	243	14

0.5 %at. Nb_2O_5 doped

JEOL

No.	2-theta	d-value	INT.	I/Io
1	21.120	4.20310	397	20
2	21.560	4.11830	252	13
3	30.560	2.92286	1957	100
4	30.880	2.89330	708	36
5	37.920	2.37077	505	26
6	43.480	2.07962	378	19
7	44.480	2.03516	343	18
8	49.240	1.84898	287	15
9	50.160	1.81720	143	7
10	54.520	1.68173	378	19
11	55.080	1.66595	470	24
12	64.240	1.44873	268	14

XRD data of PLZT (4/48/52) calcined at 950°C for 10 hours

Undoped

JEOL

No.	2-theta	d-value	INT.	I/Io
1	21.440	4.14108	441	22
2	22.000	4.03692	220	11
3	30.920	2.88965	2013	100
4	31.280	2.85721	686	34
5	38.280	2.34929	550	27
6	43.760	2.06696	389	19
7	44.880	2.01794	388	19
8	49.560	1.83779	290	14
9	50.440	1.80777	180	9
10	54.840	1.67267	452	22
11	55.600	1.65159	461	23
12	64.480	1.44392	248	12
13	65.400	1.42581	216	11

0.5 %at. Gd_2O_3 doped

JEOL

No.	2-theta	d-value	INT.	I/Io
1	21.120	4.20310	328	20
2	21.639	4.10345	225	14
3	30.600	2.91913	1641	100
4	30.960	2.88601	613	37
5	37.960	2.36836	443	27
6	43.480	2.07962	303	18
7	44.560	2.03169	354	22
8	49.280	1.84757	223	14
9	54.520	1.68173	383	23
10	55.200	1.66261	427	26
11	64.280	1.44792	259	16
12	65.120	1.43126	211	13

0.5 %at. Nb_2O_5 doped

JEOL

No.	2-theta	d-value	INT.	I/Io
1	20.960	4.23482	383	23
2	21.479	4.13365	238	14
3	30.480	2.93035	1643	100
4	30.840	2.89696	554	34
5	37.840	2.37559	454	28
6	43.360	2.08510	316	19
7	44.440	2.03690	332	20
8	49.120	1.85321	250	15
9	54.480	1.68287	359	22
10	55.120	1.66483	393	24
11	64.160	1.45034	255	16

XRD data of PLZT (5/54/46) calcined at 950°C for 10 hours

Undoped

JEOL

No.	2-theta	d-value	INT.	I/Io
1	21.079	4.21118	234	15
2	21.399	4.14892	318	20
3	30.480	2.93035	1604	100
4	30.680	2.91171	888	55
5	37.800	2.37802	438	27
6	44.280	2.04389	431	27
7	49.360	1.84476	171	11
8	54.480	1.68287	288	18
9	54.960	1.66930	461	29
10	64.120	1.45115	214	13

0.5 %at. Gd_2O_3 doped

JEOL

No.	2-theta	d-value	INT.	I/Io
1	20.960	4.23482	252	19
2	21.280	4.17185	245	18
3	30.320	2.94545	1354	100
4	30.600	2.91913	551	41
5	37.640	2.38776	312	23
6	43.320	2.08693	232	17
7	44.120	2.05093	302	22
8	49.200	1.85039	155	11
9	49.760	1.83087	120	9
10	54.280	1.68860	244	18
11	54.800	1.67380	357	26
12	63.920	1.45521	181	13
13	64.640	1.44073	176	13

0.5 %at. Nb_2O_5 doped

JEOL

No.	2-theta	d-value	INT.	I/Io
1	21.080	4.21098	320	18
2	21.440	4.14108	318	18
3	30.520	2.92660	1792	100
4	30.760	2.90431	882	49
5	37.840	2.37559	458	26
6	43.480	2.07962	272	15
7	44.280	2.04388	387	22
8	54.480	1.68287	326	18
9	54.960	1.66930	467	26
10	64.080	1.45196	247	14

APPENDIX C

Designation: C 20 – 92

Standard Test Methods for Apparent Porosity, Water Absorption, Apparent Specific Gravity, and Bulk Density of Burned Refractory Brick and Shapes by Boiling Water[1]

This standard is issued under the fixed designation C 20; the number immediately following the designation indicates the year of original adoption or, in the case of revision, the year of last revision. A number in parentheses indicates the year of last reapproval. A superscript epsilon (ε) indicates an editorial change since the last revision or reapproval.

This standard has been approved for use by agencies of the Department of Defense. Consult the DoD Index of Specifications and Standards for the specific year of issue which has been adopted by the Department of Defense.

1. Scope

1.1 These test methods cover the determination of the following properties of burned refractory brick:

1.1.1 Apparent porosity,

1.1.2 Water absorption,

1.1.3 Apparent specific gravity, and

1.1.4 Bulk density.

1.2 These test methods are not applicable to refractories attacked by water.

1.3 The values stated in inch-pound units are to be regarded as the standard. The values given in parentheses are for information only.

1.4 *This standard does not purport to address all of the safety problems, if any, associated with its use. It is the responsibility of the user of this standard to establish appropriate safety and health practices and determine the applicability of regulatory limitations prior to use.*

2. Referenced Document

2.1 *ASTM Standard:*

C 134 Test Methods for Size and Bulk Density of Refractory Brick and Insulating Firebrick[2]

E 691 Practice for Conducting an Interlaboratory Study to Determine the Precision of a Test Method[3]

3. Significance and Use

3.1 Apparent porosity, water absorption, apparent specific gravity, and bulk density are primary properties of burned refractory brick and shapes. These properties are widely used in the evaluation and comparison of product quality and as part of the criteria for selection and use of refractory products in a variety of industrial applications. These test methods are used for determining any or all of these properties.

3.2 These test methods are primary standard methods which are suitable for use in quality control, research and development, establishing criteria for and evaluating compliance with specifications, and providing data for design purposes.

3.3 Fundamental assumptions inherent in these test methods are that the test specimens are not attacked by water, the test specimens conform to the requirements for size, configuration, and original faces, the open pores of the test specimens are fully impregnated with water during the boiling treatment, and the blotting of the saturated test specimens is performed as specified in a consistent and uniform manner to avoid withdrawing water from the pores. Deviation from any of these assumptions adversely affects the test results.

3.4 Certain precautions must be exercised in interpreting and using results from these test methods. All four property values are interrelated by at least two of the three base data values generated during testing. Thus, an error in any base data value will cause an error in at least three of the property values for a given test specimen. Certain of the properties, that is, apparent specific gravity and bulk density, are functions of other factors such as product composition, compositional variability within the same product, impervious porosity, and total porosity. Generalizations on or comparisons of property values should only be judiciously made between like products tested by these test methods or with full recognition of potentially inherent differences between the products being compared or the test method used.

4. Test Specimens

4.1 When testing 9-in. (228-mm) straight brick, use a quarter-brick specimen by halving the brick along a plane parallel to the 9 by 2-½ or 3-in. (228 by 64 or 76-mm) face and along a plane parallel to the 4-½ by 2-½ or 3-in. (114 by 64 or 76-mm) face. Four of the surfaces of the resultant quarter-brick specimen include part of the original molded faces.

4.2 When testing other refractory shapes, cut, drill, or break from each shape a specimen having volume of approximately 25 to 30 in.^{3} (410 to 490 cm^3). The specimen shall include interior and exterior portions of the shape.

4.3 Remove all loosely adhering particles from each specimen.

5. Procedure

5.1 *Dry Weight, D*—Dry the test specimens to constant weight by heating to 220 to 230°F (105 to 110°C) and

---

[1] These test methods are under the jurisdiction of ASTM Committee C-8 on Refractories and are the direct responsibility of Subcommittee C08.03 on Physical Tests and Properties.

Current edition approved March 15, 1992. Published June 1992. Originally published as C 20 – 18 T. Last previous edition C 20 – 87.

[2] *Annual Book of ASTM Standards*, Vol 15.01.

[3] *Annual Book of ASTM Standards*, Vol 14.02.

determine the dry weight, D, in grams to the nearest 0.1 g.

5.2 The drying procedure may be omitted only when the test specimens are known to be dry, as may be the case with samples taken directly from kilns.

5.3 The drying of the specimens to constant weight and the determination of their dry weight may be done either before or after the saturation operation (Section 6). Usually, the dry weight is determined before saturation. However, if the specimens are friable or evidence indicates that particles have broken loose during the saturating operation, dry and weigh the specimens after the suspended weight, S, and the saturated weight, W, have been determined, as described in Sections 7 and 8. Use this second dry weight in all appropriate calculations.

6. Saturation

6.1 Place the test specimens in water and boil for 2 h. During the boiling period, keep them entirely covered with water, and allow no contact with the heated bottom of the container.

6.2 After the boiling period, cool the test specimens to room temperature while still completely covered with water. After boiling keep the specimens immersed in water for a minimum of 12 h before weighing.

7. Suspended Weight, S

7.1 Determine the weight, S, of each test specimen after boiling and while suspended in water in grams to the nearest 0.1 g.

7.2 This weighing is usually accomplished by suspending the specimen in a loop or halter of AWG Gage 22 (0.643-mm) copper wire hung from one arm of the balance. The balance shall be previously counter-balanced with the wire in place and immersed in water to the same depth as is used when the refractory specimens are in place.

8. Saturated Weight, W

8.1 After determining the suspended weight, blot each specimen lightly with a moistened smooth linen or cotton cloth to remove all drops of water from the surface and determine the saturated weight, W, in grams by weighing in air to the nearest 0.1 g. Perform the blotting operation by rolling the specimen lightly on the wet cloth, which has previously been saturated with water, and then press only enough to remove such water as will drip from the cloth. Excessive blotting will induce error by withdrawing water from the pores of the specimen.

9. Exterior Volume, V

9.1 Obtain the volume, V, of the test specimens in cubic centimetres by subtracting the suspended weight from the saturated weight, both in grams, as follows:

$$V, \text{cm}^3 = W - S \quad (1)$$

NOTE 1—This assumes that 1 cm³ of water weighs 1 g. This is true within about 3 parts in 1000 for water at room temperature.

10. Volumes of Open Pores and Impervious Portions

10.1 Calculate the volume of open pores and the volume of the impervious portions of the specimen as follows:

$$\text{Volume of open pores, cm}^3 = W - D \quad (2)$$

$$\text{Volume of impervious portion, cm}^3 = D - S \quad (3)$$

11. Apparent Porosity, P

11.1 The apparent porosity expresses as a percentage the relationship of the volume of the open pores in the specimen to its exterior volume. Calculate P as follows:

$$P, \% = [(W - D)/V] \times 100 \quad (4)$$

12. Water Absorption, A

12.1 The water absorption, A, expresses as a percentage the relationship of the weight of water absorbed to the weight of the dry specimen. Calculate A as follows:

$$A, \% = [(W - D)/D] \times 100 \quad (5)$$

13. Apparent Specific Gravity, T

13.1 Calculate the apparent specific gravity, T, of that portion of the test specimen which is impervious to boiling water as follows:

$$T = D/(D - S) \quad (6)$$

14. Bulk Density, B

14.1 The bulk density, B, of a specimen in grams per cubic centimetre is the quotient of its dry weight divided by the exterior volume, including pores. Calculate B as follows:

$$B, \text{g/cm}^3 = D/V \quad (7)$$

14.2 This test method of determining bulk density is useful for checking bulk density values obtained by direct measurement of Test Methods C 134.

NOTE 2—While it is more accurate than the direct measurement method, and generally gives higher values (by about 0.02 to 0.04), the direct measurement method is better suited for plant and field testing, since it is a less involved technique. The present method is preferable for specimens that are branded deeply or irregular in contour.

15. Report

15.1 For each property, report the individual values obtained.

15.2 Report apparent porosity and water absorption results to one decimal place, and apparent specific gravity and bulk density results to two decimal places.

NOTE 3—When values are reported for water absorption but not for porosity, it is suggested that the report shall also give the results for bulk density. This makes it possible to calculate the corresponding apparent porosity values as follows:

$$P, \% = A \times B \quad (8)$$

16. Precision and Bias

16.1 *Interlaboratory Test Data*—An interlaboratory round-robin test was conducted between six laboratories on three different types of refractories. The same four specimens of each material were sent from laboratory to laboratory, thereby eliminating sample variation. Each laboratory conducted two separate tests using two different operators, Operators A and B. The components of variance expressed as standard deviation and relative standard deviation (coefficient of variation) for absorption, apparent porosity, bulk density, and apparent specific gravity (ASG) were as given in Table 1.

TABLE 1 Interlaboratory Test Data

		Material			Grand Average
		A	B	C	
Absorption avg, %	X_j	12.37	6.67	4.83	...
Standard deviation within	S_r	0.1102	0.0776	0.075	0.0876
Standard deviation between	S_L	0.0866	0.0562	0.0182	0.0537
Relative standard deviation, %	V_r	0.89	1.16	1.55	1.20
	V_L	0.70	0.84	0.38	0.54
Apparent porosity, avg, %	X_j	22.24	14.44	11.22	...
	S_r	0.1893	0.1559	0.1696	0.1716
	S_L	0.0000	0.0000	0.0000	0.0000
	V_r	0.85	1.08	1.51	1.15
	V_L	0.00	0.00	0.00	0.00
Bulk density, avg	X_j	1.799	2.172	2.327	...
	S_r	0.00189	0.00458	0.00206	0.00284
	S_L	0.00274	0.00296	0.00267	0.00279
	V_r	0.105	0.211	0.089	0.135
	V_L	0.152	0.136	0.115	0.134
Apparent specific gravity, avg	X_j	2.314	2.539	2.621	...
	S_r	0.00577	0.00634	0.00495	0.00569
	S_L	0.00442	0.00468	0.00438	0.00449
	V_r	0.249	0.250	0.189	0.229
	V_L	0.191	0.184	0.167	0.181

TABLE 2 Precision and Relative Precision

Test Property	Precision		Relative Precision	
	Repeatability, I_r	Reproducibility I_R	% I_r	% I_R
Absorption, %	0.25	0.29	3.40	3.9
Apparent porosity, %	0.49	0.49	3.25	3.25
Bulk density	0.008	0.011	0.38	0.54
Apparent specific gravity	0.016	0.021	0.65	0.83

NOTE 4—All statistical calculations are in accordance with Practice E 691.

16.2 *Precision*—For the components of variation given in 16.1, a test result on any one sample should be considered significantly different at a confidence level of 95 %, if the repeatability used for reproducibility exceeds the precision data given in Table 2.

16.3 *Bias*—No justifiable statement on bias is possible since the true physical property values of refractories cannot be established by an accepted reference material.

17. Keywords

17.1 apparent porosity; apparent specific gravity; bulk density; refractory shapes; water absorption; water boil

Vita

Mr. Bhanu Vetayanugul was born on August 23, 1978 in Bangkok. He obtained a bachelor's degree of Science in physics at Chulalongkorn University in 1999. He began his master's study in March 1999 at the Department of Materials Science, Chulalongkorn University and completed the program in May 2001. He has won the Best Poster Award at 26th Congress on Science and Technology of Thailand in October 2000.